Chapter 2
Porous Carbons for Carbon Dioxide Capture

An-Hui Lu, Guang-Ping Hao and Xiang-Qian Zhang

Abstract Porous carbons play an important role in CO_2 adsorption and separation due to their developed porosity, excellent stability, wide availability, and tunable surface chemistry. In this chapter, the synthesis strategies of porous carbon materials and evaluation of their performance in CO_2 capture are reviewed. For clarity, porous carbons are mainly classified into the following categories: conventional activated carbons (ACs), renewable-resources-derived porous carbons, synthetic polymer-based porous carbons, graphitic porous carbons, etc. In each category, macroscopic and microscopic morphologies, synthesis principles, pore structures, composition and surface chemistry features as well as their CO_2 capture behavior are included. Among them, porous carbons with targeted functionalization and a vast range of nanostructured carbons (carbon nanofibers, CNTs, graphene, etc.) for CO_2 capture are being created at an increasing rate and are highlighted. After that, the main influence factors determining CO_2 capture performance including the pore features and heteroatom decoration are particularly discussed. In the end, we briefly summarize and discuss the future prospectives of porous carbons for CO_2 capture.

2.1 Introduction

The term "Carbon Filter Process (CFP)" has been proposed and accepted widely. Selected carbonaceous materials, e.g., activated carbons (ACs), carbon aerogels, and carbon fibers, act as filter materials, which deliver a high affinity (and, hence, high capacity) to CO_2 but not to its balance gas. This, in turn, leads to a high selectivity of CO_2/balance gas (in most case, N_2). Most importantly, along with the improvement in science and technology, it has been possible to synthesize carbon materials with

A.-H. Lu (✉) · G.-P. Hao · X.-Q. Zhang
State Key Laboratory of Fine Chemicals, School of Chemical Engineering, Dalian University of Technology, Dalian 116024, People's Republic of China
e-mail: anhuilu@dlut.edu.cn

A.-H. Lu and S. Dai (eds.), *Porous Materials for Carbon Dioxide Capture*, Green Chemistry and Sustainable Technology, DOI: 10.1007/978-3-642-54646-4_2,

defined nanostructure and morphology, tunable surface area, and pore size. Because of the advanced porous carbon materials, current CFP can recover more than 90 % of flue gas CO_2 (with purity of higher than 90 %) at a fraction of the cost normally associated with the conventional amine absorption process.

2.2 Conventional Activated Carbons (ACs) for CO_2 Capture

ACs are the most commonly used form of porous carbons for a long time. Typically, they refer to coal and petroleum pitch as well as coconut shells-based AC. In most cases, ACs are processed to be filled with rich micropores that increase the surface area available for gas sorption and separation. For this category, to get a definite classification on the basis of pore structure is difficult due to their countless products as well as their complex pore features. Based on the physical characteristics, they can be widely classified into the following types: powdered, granular, extruded, bead ACs, etc. For the pore structure of ACs, actually, all the three types of pores (micropore, mesopore, and macropore) are included in one product (Fig. 2.1), with a wide pore size distribution [1, 2]. Up to now, many kinds of ACs have been well commercialized in gas sorption/separation including CO_2 capture. For example, the BPL type with specific area of 1,141 $m^2\ g^{-1}$ is able to adsorb 7 mmol g^{-1} CO_2 under the conditions of 25 °C and 35 bar, while under the same conditions MAXSORB-activated carbon with specific area of 3,250 $m^2\ g^{-1}$ can capture up to 25 mmol g^{-1} [3].

2.3 Renewable-Resources-Derived Porous Carbons for CO_2 Capture

New types of porous carbons for CO_2 capture have been created through carbonization and activation of renewable biomass precursors, such as coconut husk, bamboo, wood, peat, cellulose, and lignite due to their wide availability and renewable features (Fig. 2.2). Interestingly, for this category, as new precursors are discovered, new types of ACs can be created through carbonization and activation. For example, the precursors can be extended to microorganism, celtuce leaves, fungi, algae, bean dreg, and so on [4–6]. And thus such carbon "family" is enriched and will be further expanded due to the widely available carbon precursors and their high effectiveness in CO_2 capture.

2.3.1 Direct Pyrolysis Method

Direct pyrolysis combined with activation of renewable biomass precursors has been widely studied and employed for fabricating the porous carbon materials. For example, waste celtuce leaves were used to prepare porous carbons by air-drying,

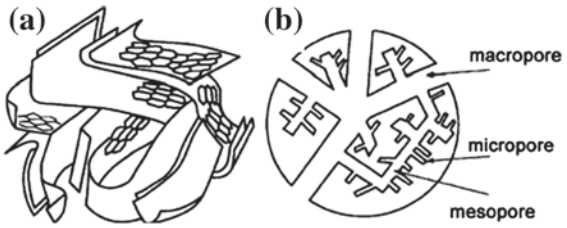

Fig. 2.1 Schematic representation three-dimensional (**a**) and two-dimensional (**b**) structures of the ACs. Reprinted from Ref. [1], Copyright 1998, with permission from Elsevier

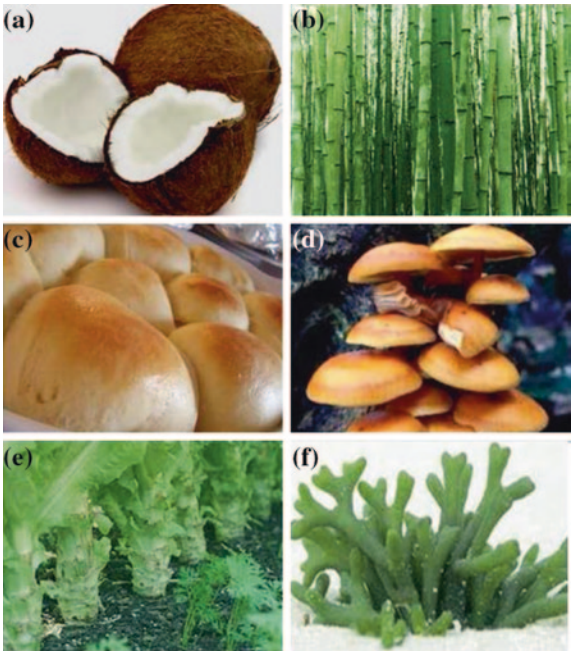

Fig. 2.2 Biomass feed stocks as carbon precursors: **a** coconut shell; **b** bamboo; **c** yeast; **d** fungi; **e** celtuce leaves; and **f** algae

pyrolysis at 600 °C in argon, followed by KOH activation. The as-prepared porous carbons show a very high specific surface area of 3,404 $m^2\ g^{-1}$ and a large pore volume of 1.88 $cm^3\ g^{-1}$. They show an excellent CO_2 adsorption capacity at 1 bar, which is up to 6.04 and 4.36 mmol g^{-1} at 0 and 25 °C, respectively. Wang et al. [7] reported a series of porous carbons with adjustable surface areas and narrow micropore size distribution by KOH activation of fungi-based carbon sources. The high CO_2 uptake of 5.5 mmol g^{-1} and CO_2/N_2 selectivity of 27.3 at 1 bar, 0 °C of such fungi-based carbons made them promising for CO_2 capture and separation. Similarly, Shen et al. [8] found that yeast is a promising carbon precursor for the synthesis of hierarchical microporous carbons, which show a high CO_2 adsorption capacity (4.77 mmol g^{-1}) and fast adsorption rate (equilibrium within 10 min) at 25 °C. This may stem from their large surface area and hierarchical pore systems as well as the surface-rich basic sites.

Table 2.1 Porosity characterization of the carbon monoliths selected in the present study, deduced from N_2 (–196 °C) and CO_2 (0 °C) adsorption isotherms and densities of the carbon monoliths

Monolith	S_{BET} ($m^2\ g^{-1}$)	V_{DR} (N_2) ($cm^3\ g^{-1}$)	V_{DR} (CO_2) ($cm^3\ g^{-1}$)	Density ($g\ cm^{-3}$)
A1	928	0.43	0.44	1.00
A3	941	0.43	0.45	1.07
A3–12	988	0.56	0.50	0.99
A3–24	1,145	0.66	0.57	0.93
A3–36	1,367	0.71	0.50	0.87
A3–48	1,586	0.77	0.50	0.80
M3	3,180	1.31	0.70	–
K1	3,120	1.25	0.72	–
M3M	2,610	0.93	0.60	0.42
K1M	2,320	0.91	0.59	0.50

Reproduced from Ref. [9] by permission of The Royal Society of Chemistry

Different from microstructure tuning, their macrostructures (form, density, etc.) modification is also crucial for reducing pressure drop, mitigating adsorption heat as well as enhancing volumetric capture capacity. Linares-Solano et al. [9] systematically investigated this issue by using carefully selected carbon monoliths (A series, M3M and K1M). The properties of the three types are characterized and compared in their work. As seen, A series monoliths show high-density values but moderate porosities, while M3M and K1M represent the other type with moderate densities and high porosity developments (Table 2.1).

From the systematical CO_2 adsorption investigation, the authors found that (1) the gravimetric storage capacities of the adsorbents depend on their textural properties, while the volumetric adsorption capacity is directly related to their textural properties and densities. It is worth to note that the density shows the most important impact on gas storage capacity. (2) due to their singular high density, the A series carbon monoliths, as well as its CO_2 activated carbon monoliths, present exceptionally high volumetric storage capacity for CO_2 at room temperature.

In parallel with the structure tuning, the carbon surface properties can also be modified by selecting the N-containing precursors [6, 10]. For example, Xing et al. [6] prepared a series of N-doped ACs from bean dreg by KOH activation and investigated their CO_2 capture properties. The resulting materials possess a very high CO_2 uptake of up to 4.24 mmol g^{-1} at 25 °C under 1 atm. They demonstrated that the CO_2 uptake is independent of the specific surface area and micropore volume, but closely related to the N content of the ACs. In their opinion, the introduction of N into a carbon surface facilitates the hydrogen-bonding interactions (Fig. 2.3) between the carbon surface and CO_2 molecules rather than the acid–base interactions between N-containing basic functional groups and acidic CO_2 molecules, which accounts for the superior CO_2 uptake of the N-doped porous carbons.

Similarly, Sevilla et al. [11] reported a chemical activated synthesis (KOH as activating agent) of highly porous N-doped carbons for CO_2 capture. In their synthesis method, polypyrrole (PPy) was selected as carbon precursor. The activation process was carried out under severe (KOH/PPy = 4) or mild (KOH/PPy = 2)

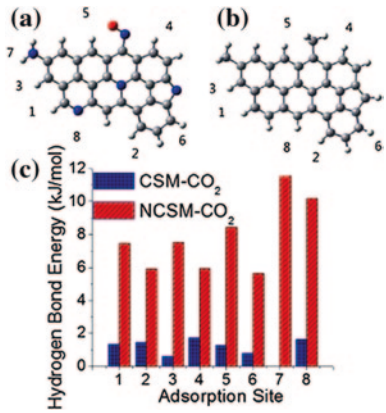

Fig. 2.3 Theoretical models for **a** N-doped carbon surface and **b** pure carbon surface (*red ball* oxygen atom; *blue ball* nitrogen atom; *gray ball* carbon atom; *small gray ball* hydrogen atom). **c** Hydrogen bond energies at different adsorption sites. Reproduced from Ref. [6] by permission of The Royal Society of Chemistry

activation conditions at different temperatures in the 600–800 °C range. Mildly activated carbons have two important characteristics: (1) they contain a large number of nitrogen functional groups (up to 10.1 wt% N) identified as pyridonic-N with a small proportion of pyridinic-N groups, and (2) they exhibit, in relation to the carbons prepared with KOH/PPy = 4, narrower micropore size. The above two properties ensure the mildly activated carbons a large CO_2 adsorption capacities. Furthermore, the capture of CO_2 over this type of carbon takes place at high adsorption rates, more than 95 % of the CO_2 being adsorbed in ca. 2 min. In contrast, N_2 adsorption occurs at slower rates; approximately 50 min are necessary to attain maximum adsorption uptake (0.77 mmol N_2 g^{-1}).

2.3.2 Sol-gel Process and Hydrothermal Carbonization Method

Another new but rapidly expanding research area is the production of porous carbons from renewable resources (e.g., collagen, cellulose, and starch) based on a sol-gel process (Fig. 2.4) [12, 13]. One of the successful examples is polysaccharide-derived "Starbons®" carbon, which exhibits outstanding mesoporous textural properties. More importantly, their pore volumes and sizes are comparable to materials prepared via the hard template routes or soft template methods based on the self-assembly and polymerization of aromatic precursors (e.g., phenols). In this technology, three main stages are involved. Selected precursors are first gelatinized by heating in water. Then, the water inside of the gel is exchanged with the lower surface tension solvent (e.g., ethanol). After drying, the porous gel is doped with a catalytic amount of acid and pyrolyzed under vacuum, ending up in highly porous carbons.

Sol-gel method is indeed a simple and direct approach for the synthesis of bulky carbons and is already widely used in both laboratory and industry. However, the major disadvantage is the long synthesis period and the rigorous drying process of

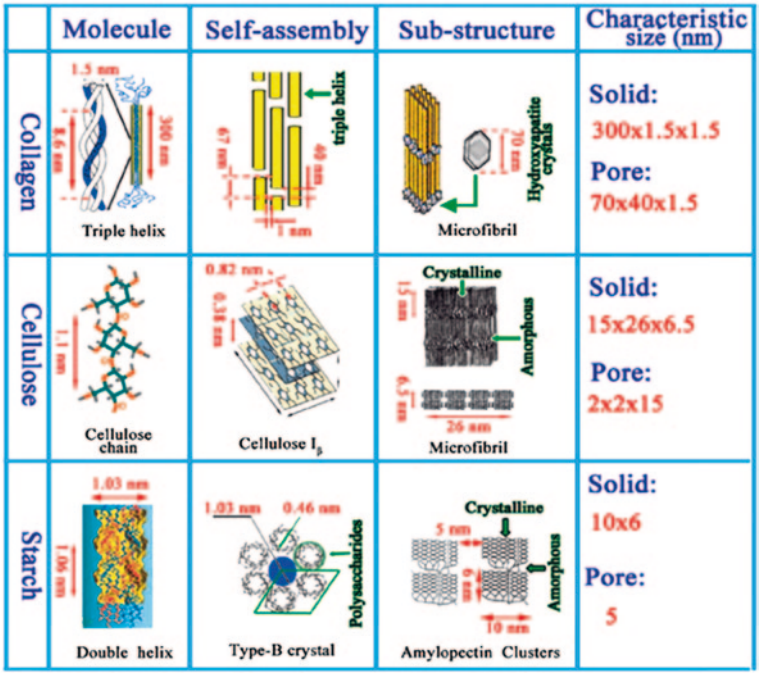

Fig. 2.4 Examples of organized hierarchical structures found in biological systems. Reproduced from Ref. [12] by permission of The Royal Society of Chemistry

the wet gel (i.e., solvent exchange or supercritical drying), in which slight variations may cause drastic variations in the structural features, and hence properties [14]. In addition, pore blocking and sometimes uncontrolled dispersion of active sites both on the surface and in carbon pore walls remain to be solved.

Concurrently with the "Starbons ®" technology, Titirici et al. [15, 16] have been particularly active in the development and production of useful carbonaceous materials from sugar-based biomass via a hydrothermal carbonization (HTC) approach. HTC is a spontaneous, exothermic process, producing materials where the majority of the original carbons are incorporated into the final structure. The initial products of the sugar dehydration (e.g., furfuryl derivatives) are thought to polymerize to form condensed spherical functional carbons after autoclave processing at 180 °C for 20–24 h (Fig. 2.5) [17]. Manipulation of particle size was possible via the utilization of different sugar-based carbon sources, while the surface and bulk chemical structure of the material may be directed by the utilization of hexose- or pentose-based biomass, as demonstrated by ^{13}CP MAS NMR investigations [16]. HTC is relatively straightforward, affording small colloidal carbon spheres (CS), the surface texture and chemistry of which can be controllable via the introduction of co-monomers, and selection of biomass precursor. However, HTC materials demonstrate low or negligible surface areas, very small particle size, and little developed or structured porosity.

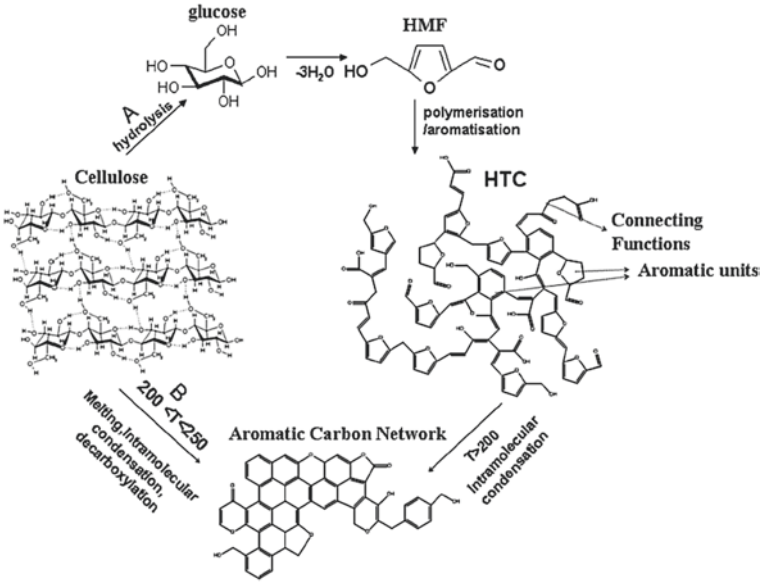

Fig. 2.5 Conversion of cellulose into HTC: A via HMF resulting in a furan-rich aromatic network and B direct aromatization. Reproduced from Ref. [17] by permission of The Royal Society of Chemistry

The CO_2 capture behavior over HTC-based porous carbons has recently been investigated. For example, Sevilla and Fuertes [18] reported a series of sustainable porous carbon capture materials, which are produced from the chemical activation of hydrothermally treated precursors (polysaccharides and biomass) using KOH as an activating agent. The CO_2 adsorption properties, kinetics, and regeneration of these materials were investigated. Compared with the raw HTC materials, the chemical activated counterparts show a significant increase of micropores, delivering a high surface area of 1,260 and 2,850 $m^2\ g^{-1}$ depending on the activation conditions. The CO_2 capture properties at 0, 25, and 50 °C and 1 bar are studied. As shown in Fig. 2.6, these HTC-based porous carbons show a high capacity even up to 4.8 mmol g^{-1} at 25 °C and 1 atm. They found that the remarkable CO_2 capture capacity arises from the presence of rich and narrow micropores (<1 nm), and the surface area plays a less important role. More interestingly, they found that this type of porous carbons showed very fast adsorption kinetics. Around 95 % CO_2 uptake can be achieved in 2 min. Under the same conditions, the N_2 adsorption uptake is 1/9 of that of CO_2, indicating a CO_2/N_2 selectivity of ca. 9.

Subsequently, Sevilla et al. [19] prepared the highly porous N-doped carbons through chemical activation of hydrothermal carbons derived from mixtures of algae and glucose. They demonstrate that the control of the activation conditions (temperature and amount of KOH) allows the synthesis of exclusively microporous biomass-based materials. These materials possess surface areas in the range of 1,300–2,400 $m^2\ g^{-1}$ and pore volumes up to 1.2 $cm^3\ g^{-1}$. They additionally exhibit

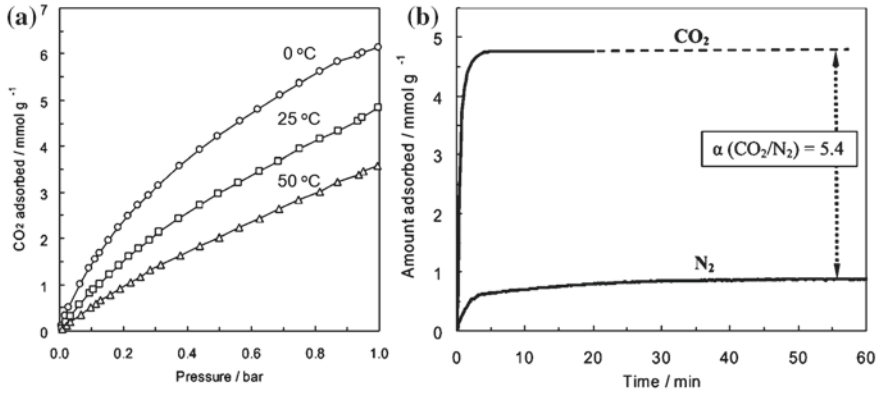

Fig. 2.6 **a** CO_2 adsorption isotherms at 0, 25, and 50 °C and **b** adsorption kinetics of CO_2 and N_2 at 25 °C for the HTC-based porous carbons AS-2-600 sample. Reproduced from Ref. [18] by permission of The Royal Society of Chemistry

the N contents in the range of 1.1–4.7 wt%, and these heteroatoms being mainly present as pyridone-type structures. When tested as CO_2 sorbents at subatmospheric conditions, they show a large CO_2 capture capacity of up to 7.4 mmol g^{-1} at 0 °C and 1 bar, which is among the highest values for porous materials. However, the results indicate that the large CO_2 capture capacity is exclusively due to their high volume of narrow micropores and not to the high surface areas or pore volumes, neither to the presence of heteroatoms.

2.4 Synthetic Polymer-Based Porous Carbons for CO_2 Capture

Compared with conventional ACs and biomass-derived carbons, the use of synthetic polymers as porous carbons precursors enables better chemical composition control, easy-to-achieve precise morphology, tunable pore system, and targeted surface chemistry. Thus, synthetic polymers-based porous carbons are extensively investigated nowadays. The strategies toward advanced porous carbons mainly rely on protocols such as precursor-controlled pyrolysis, rational synthesis by chemical vapor deposition (CVD), templating and surface-mediated synthesis, self-assembly, surface-grafting and modification, and others. The CO_2 capture performances are strongly depending on these microstructure features. This can be achieved by a designed synthesis methodology. Thus, a precise controlled synthesis on carbon structure will provide a promising opportunity to authentically understand the physical and chemical properties of carbon materials from molecular level and thereby efficiently guide practical applications. For clarity, in this part, the porous carbon materials are classified into the following groups according to synthesis methods: template-free synthesis, self-assembly strategy, and hard template method. In each group, several subgroups

are further included according to their morphologies: 3D monolithic structure, 2D films, membranes, and spheres. To note, ionic liquids or related derivates derived porous carbons have been discussed in Chap. 1 and thus are not within the scope here.

2.4.1 Template-Free Synthesis

2.4.1.1 Monoliths

Porous carbons are versatile materials that possess a wide range of morphologies not only on the microscopic level but also on the macroscopic level. Macroscopically, a monolith generally shows wide flexibility of operation in contrast to its powder counterparts [20]. Microscopically, monolithic structure is characterized by its 3D bicontinuous hierarchical porosity, which usually leads to several distinct advantages such as low pressure drop, fast heat and mass transfer, high contacting efficiency, and easy to deal with [21–24]. Thus, the monolithic carbons well apply to gas sorption and separation, including CO_2 capture.

The synthesis of monolithic carbons generally relies on the means including sol-gel method and self-assembly approach [25, 26]. In recent years, much efforts have been devoted to create new types of carbon monoliths with enhanced functions, which are developing new polymerization systems (solvents and/or precursors), precise pore engineering toward multimodal porosities, and targeted surface/bulk functionalization for a high performance in CO_2 capture [27–30].

The sol-gel method is one of the most conventional methods to prepare bulk carbon materials with fully interconnected pores. Carbon aerogels are the representative monolithic materials, whose synthesis generally involves the transformation of molecular precursors into highly cross-linked organic gels based on sol-gel chemistry [31]. Since the pioneering work of Pekala [32], the polymer-based monolithic carbons have scored remarkable achievements in the new polymerization system and further surface/bulk functionalization. Fairén-Jiménez et al. [33] synthesized carbon aerogels with monolith density ranging from 0.37 to 0.87 g cm^{-3} by carbonization of organic aerogels deriving from resorcinol–formaldehyde (RF) polymer prepared in various solvents such as water, methanol, ethanol, tetrahydrofuran, or acetone solution. They found that the samples with a density higher than 0.61 g cm^{-3} had micropores and mesopores but no macropores.

Using deep eutectic salts either as solvents, or as carbonaceous precursors and structure-directing agents, Monte's group prepared carbon monoliths with high yield (80 %) and tailored mesopore diameters [34, 35]. Sotiriou-Leventis, and coworkers, in recent years, have developed several new polymerization systems such as isocyanate-cross-linked RF gels, polyurea (PUA) gels, and polyimide gels, which offer a high degree of flexibility in producing the monolithic carbons [36–38]. The carbon products show interconnected hierarchical pore networks and 3D bicontinuous morphology, high surface area, and large pore volume. For example, PUA gels, which eventually convert to highly porous (up to 98.6 % v/v) aerogels

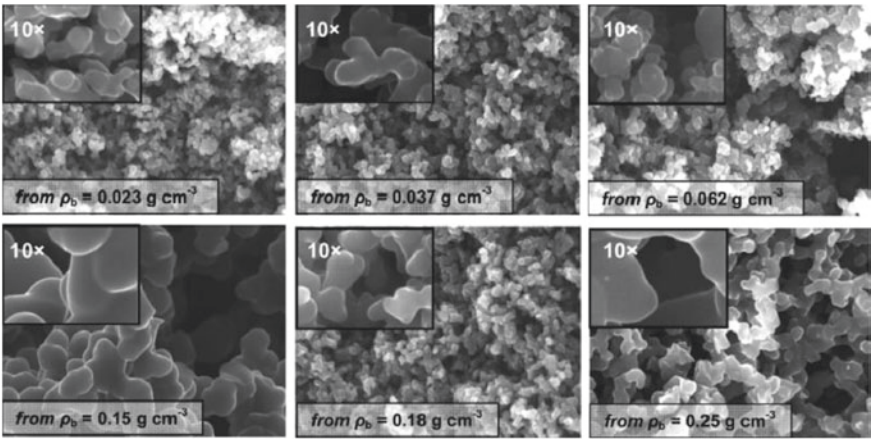

Fig. 2.7 SEM of carbon aerogels derived from **polyurea** aerogels made of Desmodur RE triisocyanate. Densities (*inset*) are those of the parent **polyurea** aerogels. Scale bar: 5 μm. Densities of the actual C samples (from *left* to *right*): *top row*, not measured (sample broke to pieces); 0.29 ± 0.06 g cm^{-3}; 0.40 ± 0.02 g cm^{-3}; *lower row*, 0.62 ± 0.08 g cm^{-3}; 0.72 ± 0.03 g cm^{-3}; 0.78 ± 0.01 g cm^{-3}). Reprinted with the permission from Ref. [36]. Copyright 2010 American Chemical Society

over a very wide density range, can be prepared by carefully controlling of the relative Desmodur RE (isocyanate)/water/triethylamine (catalyst) ratios in acetone (Fig. 2.7). It is worthy of exploration of their applications as CO_2 capture materials in the forthgoing research.

Alternatively, the copolymerization and/or cooperative assembly between carbon precursors, and one or more additional modifiers (i.e., heteroatom-containing components), can be used to directly synthesize functional carbons with enhanced CO_2 adsorption capability [39]. Sepehri et al. [40] synthesized a series of nitrogen–boron codoped carbon cryogels by homogenous dispersion of ammonia borane in RF hydrogel during solvent exchange and followed by freeze-drying and pyrolysis. The nitrogen–boron codoping results in a big improvement in porous structure and thus accelerates molecule/ions transport properties as compared to the non-modified carbons. Recently, Lu's group reported a time-saving synthesis toward to a new type of nitrogen-doped carbon monolith through a sol-gel copolymerization of resorcinol, formaldehyde, and L-lysine [41]. Based on N_2 sorption, TEM and SEM results (Fig. 2.8), it is clear that this carbon monolith possesses a hierarchical porous structure, i.e., contains both macropores and micropores. This should be advantageous for a CO_2 sorption process, since the macropores provide low-resistant pathways for the diffusion of CO_2 molecules, while the micropores are most suitable for trapping of CO_2.

As expected, such a monolithic carbon performs very well in CO_2 capture with the capacity of 3.13 mmol g^{-1} at 25 °C. With an increase in adsorption temperature, the adsorption capacities decrease from 3.13 to 1.64, 1.22 to 0.62 mmol g^{-1}, at the corresponding temperatures of 60, 80, and 120 °C, but are still at a high level

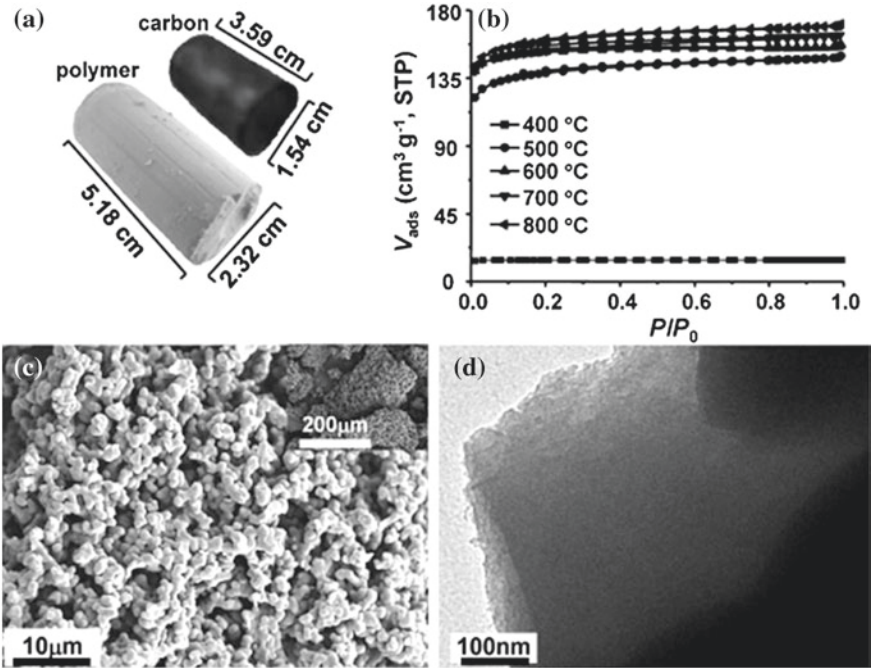

Fig. 2.8 **a** Photograph of as-made polymer monolith and its carbonized product. **b** N_2-sorption isotherms of the obtained carbon monolithic pyrolyzed at different temperatures (P/P_0 is the relative pressure). **c**, **d** SEM and TEM images of sample carbonized at 500 °C (the *inset* in c) show an overview of the macroscopic structure. Reproduced from Ref. [41] by permission of John Wiley & Sons Ltd

as compared to its non-doped analogous carbon monoliths (Fig. 2.9). Also to note, the decrease in the CO_2 adsorption capacity at high temperature is the common effect of porous carbons. The high uptake at the initial stage of the isotherm may be attributed to the affinity between basic nitrogen groups and CO_2 via acid–base interaction. Interestingly, they undergo an easy regeneration process, i.e., by argon purge at room temperature.

2.4.1.2 Spheres

Dimensionally, porous carbons can also be processed into size-shortened spheres. Commonly, carbon-based spheres are prepared by carbonization of polymer analogs. In this case, polymer precursors are required to be thermally stable and are able to form carbon residue after a high-temperature pyrolysis. Phenolic resins derived from the polymerization of phenols (e.g., phenol, resorcinol, phloroglucinol) with aldehyde (e.g., formaldehyde, furfuraldehyde, hexamethylenetetramine) are attractive due to their excellent performance characteristics such as high-temperature

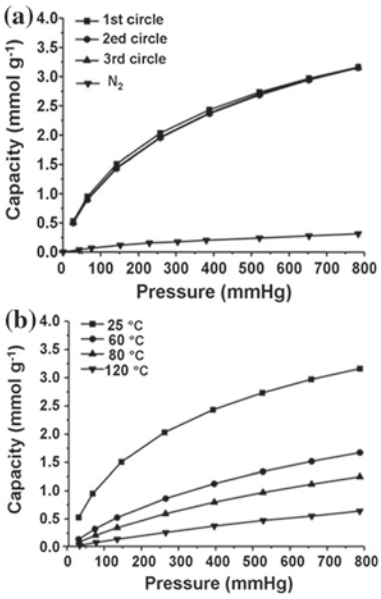

Fig. 2.9 **a** CO_2 multicircle sorption isotherms and N_2 sorption isotherm for sample at 25 °C, **b** temperature-dependent CO_2 adsorption isotherms at 25, 60, 80, and 120 °C. Reproduced from Ref. [41] by permission of John Wiley & Sons Ltd

resistance, thermal abrasiveness, and high yield of carbon conversion. As a result, varieties of chemical syntheses have been reported for the preparation and CO_2 adsorption performance of CS [42–46].

Yuan et al. [47] reported a new type of spherical nitrogen-containing polymer and microporous carbon materials for CO_2 adsorption analysis. In their synthesis, a nitrogen-containing compound, hexamethylenetetramine, was selected as both a nitrogen source and one of the carbon precursors under solvothermal conditions, without using any surfactant or toxic reagent such as formaldehyde. Thus, the synthesis strategy is user-friendly, cost-effective and can be easily scaled up for production. The microporous CS exhibit high surface areas of 528–936 $m^2\ g^{-1}$ with a micropore size of 0.6–1.3 nm. The synthesized microporous carbons show a good CO_2 capture capacity, which is mainly due to the presence of nitrogen-containing groups and a large amount of narrow micropores (<1.0 nm). At 1 atm, the equilibrium CO_2 capture capacities of the obtained microporous carbons are in the range of 3.9–5.6 mmol g^{-1} at 0 °C and 2.7–4.0 mmol g^{-1} at 25 °C.

Further, they normalized the CO_2 capture capacities in accordance with narrow micropore volume and nitrogen content, with the aim to determine the influence of both textural and surface chemistry properties on their capture performance. The normalization of the CO_2 capture capacities by the narrow micropore volume shows the effect of surface chemistry properties of the samples on the CO_2 uptake, while the normalization by nitrogen content exhibits the contribution of textural properties. From the results, we can assume that samples prepared from low treatment temperature (i.e., 600 °C) exhibit the greatest capacity per narrow micropore volume, while high-temperature pyrolyzed samples show increased contribution by the micropores.

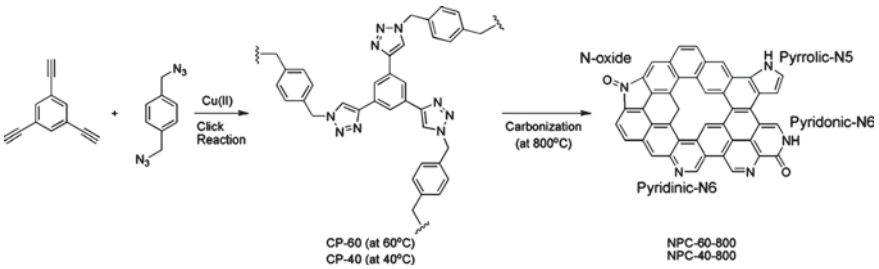

Fig. 2.10 Synthetic scheme for the N-doped porous carbon materials. Several key nitrogen species are indicated in NPC materials. Reprinted from Ref. [48]. Copyright 2013, with permission from Elsevier

Gu et al. [48] have developed a template-free synthesis for new types of porous CS, which show a good performance in CO_2 capture. In their synthesis, the azide–alkyne 1,3-dipolar Huisgen cycloaddition reaction was employed for the condensation of 1,4-bis(azidomethyl)benzene and 1,3,5-ethynylbenzene (Fig. 2.10). Because the resulting solid product contains periodically arranged aromatic 1,2,3-triazole rings in the polymer backbone, such carbon precursors contain a large percentage of nitrogen atom sources for the preparation of N-doped carbon materials. More importantly, it may be possible to control the N-doping level of products by simply changing the degree of polymerization for the carbon precursors. As expected, the N contents and surface area can be tuned to 4.30 wt% and 423 $m^2\ g^{-1}$ after a pyrolysis under 800 °C. Based on the developed pores and high N content, the sample can adsorb 126.8 $cm^3\ g^{-1}$ (5.66 mmol g^{-1}), 69.6 $cm^3\ g^{-1}$ (3.10 mmol g^{-1}), and 53.9 $cm^3\ g^{-1}$ (2.41 mmol g^{-1}) of CO_2 at 196, 273, and 298 K, respectively.

2.4.2 Self-assembly Method

2.4.2.1 Monolith

Imparting mesoscale pores is an effective way to enhance sorption kinetics, which can go beyond that of microporous ACs. Particularly, mesoporous carbons with defined pore size and symmetry provide a possibility for the fabrication of model carbons, which are highly valuable for fundamental investigation of the adsorption processes. Thus, besides the porous carbon monoliths showing irregular mesopores, great progress has also been achieved in the synthesis of monolithic carbons with ordered mesoporosity by self-assembly of copolymer molecular template and carbon precursors. However, it remains a great challenge to achieve highly developed mesoporosity while to remain good monolith morphology due to the following requirements. Firstly, a perfect matching interaction between the carbon-yielding precursors and the pore-forming component is required, which allows self-assembling of a stable micelle nanostructure; secondly,

the micelle structures should be stable during sustaining the temperature required for curing a carbon-yielding component, but can be readily decomposed during carbonization; thirdly, the carbon-yielding component should be able to form a highly cross-linked polymeric materials that can retain their nanostructure during the decomposition or the extraction of the pore-forming component. In order to achieve a monolithic carbon with well-developed mesoporosity, not a single one of these conditions can be dispensed with.

Dai's group first synthesized highly ordered mesoporous carbon through a solvent annealing accelerated self-assembly method using polystyrene-block-poly(4-vinylpyridine) (PS-P4VP) as soft templates and *N*,*N*-dimethylformamide (DMF) as solvent [49]. However, the samples are in film form. Since then, using self-assembly method to prepare porous carbons has been extensively investigated. At present, the products are mostly in a form of powder or film. For example, Valkama et al. [50] reported a soft template method to achieve carbon products in any desired shape, and the porosity can be tuned from mesoporous to hierarchically micro- and mesoporous simply by varying pyrolysis conditions for the cured block copolymer–phenolic resin complexes.

Recently, based on the soft-templating principle, Dai's group reported a versatile synthesis of porous carbons (monolith, film, fiber, and particle) by using phenol-, resorcinol-/phloroglucinol-based phenolic resins as carbon precursors and triblock copolymer (F127) as the soft template. They found that due to the enhanced hydrogen-bonding interaction with triblock copolymers, phloroglucinol with three hydroxyl groups is an excellent precursor for the synthesis of mesoporous carbons with well-organized mesostructure [51]. This type of mesoporous carbon monolith shows good performance in gas capture [52]. At 800 Torr and 298 K, the adsorption equilibrium capacity of the ordered mesoporous carbon for CO_2 is 1.49 mmol g^{-1}. Significantly higher adsorption uptake was observed for CO_2 to be 3.26 mmol g^{-1} at 100 bar and 298 K. More interestingly, the diffusion time constant of CO_2 decreased with adsorbate pressures due to the obvious mesoscale pore system.

Later, they prepared carbons with ordered mesopores based on self-assembly approach of RF polymer and block copolymers under strong acidic conditions and by subsequent centrifugation and shaping techniques. The $I^+X^-S^+$ mechanism and hydrogen bonding are believed to be the driving force for self-assembly between the RF resol and F127 template [53]. The polymerization-induced spinodal decomposition in glycolic solutions of phloroglucinol/formaldehyde polymers and block copolymers also leads to successful formation of the bimodal meso-/macroporous carbon monoliths [54].

Alternatively, Zhao's group developed a hydrothermal synthesis by using F127 and P123 as double soft templates and phenol/formaldehyde as carbon precursor (molar ratio between phenol and surfactant about 46:1), followed by hydrothermal aging at 100 °C for 10 h [55]. Recently, the same group reported a controllable one-pot method to synthesize N-doped ordered mesoporous carbon with a high N content by using dicyandiamide as a nitrogen source via an evaporation-induced self-assembly process [56]. In this synthesis, resol molecules can bridge the Pluronic F127 template and dicyandiamide via hydrogen-bonding and electrostatic

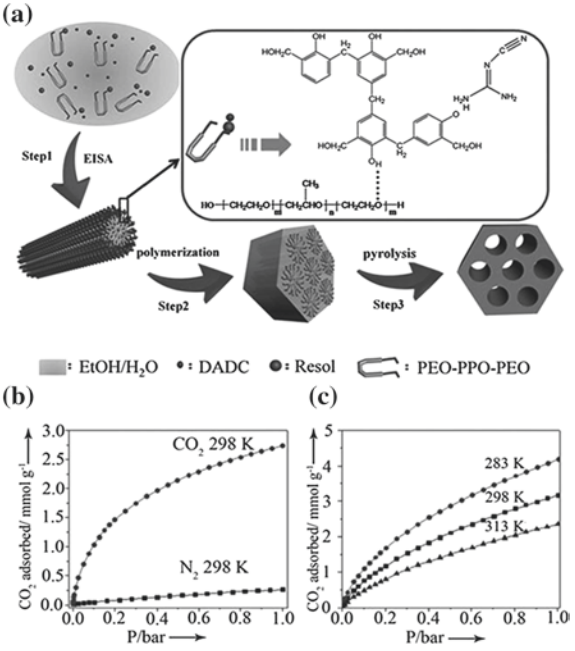

Fig. 2.11 **a** The formation process of ordered N-doped mesoporous carbon from a one-pot assembly method using dicyandiamide (DCDA) as a nitrogen source. **b** CO_2 and N_2 adsorption isotherms at 25 °C for the N-doped mesoporous carbon H-NMC-2.5. **c** CO_2 adsorption isotherms at different temperature for A-NMC after activation by KOH. Reproduced from Ref. [56] by permission of John Wiley & Sons Ltd

interactions. During thermosetting at 100 °C for formation of rigid phenolic resin and subsequent pyrolysis at 600 °C for carbonization, dicyandiamide provides closed N species, while resol can form a stable framework, thus ensuring the successful synthesis of ordered N-doped mesoporous carbon (Fig. 2.11). Such N-doped ordered mesoporous carbons possess tunable mesostructures (p6m and Im3m symmetry) and pore size (3.1–17.6 nm), high surface area (494–586 $m^2\ g^{-1}$), and high N content (up to 13.1 wt%). Ascribed to the unique feature of large surface area and high N contents, the materials show high CO_2 capture of 2.8–3.2 mmol g^{-1} at 25 °C and 1.0 bar (Fig. 2.11).

Similarly, Xiao's group also reported a hydrothermal synthesis at even higher temperature and longer time (i.e., 260 °C for more than 17 h) to prepare carbon monoliths with well-ordered hexagonal or cubic mesopore systems [57]. Meanwhile, Gutiérrez et al. [58] synthesized a low-density monolithic carbon exhibiting a 3D continuous micro- and macroporous structure, which derived from a PPO_{15}-PEO_{22}-PPO_{15} block copolymer-assisted RF polymerization. Zhang's group reported an organic–organic aqueous self-assembly approach to prepare B-/P-doped ordered mesoporous carbons using boric acid and/or phosphoric acid as B- or P-heteroatom source, RF resin as the carbon precursor and triblock copolymer Pluronic F127 as the mesoporous structure template [59]. Lu's group established a rapid and scalable synthesis of crack-free and nitrogen-doped carbon monolith with fully interconnected macropores and an ordered mesostructure through the soft template method. The monolith is achieved by using organic base lysine as a polymerization agent and mesostructure assembly promotor, through

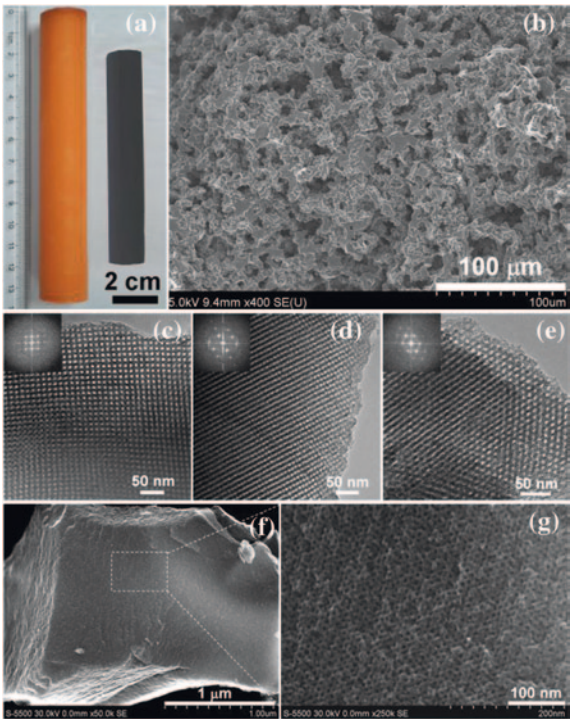

Fig. 2.12 Photograph of the synthesized polymer and carbon monolith (**a**); SEM images of carbon monolith HCM-DAH-1 (**b**); TEM images (**c**, **d**, and **e**: images viewed in the [100, 110, 111] direction; the insets are the corresponding fast Fourier transform (FFT) diffractograms) and HR-SEM images (**f**, **g**) of the carbon monolith HCM-DAH-1. Reprinted with the permission from Ref. [61]. Copyright 2011 American Chemical Society

rapid sol-gel process at 90 °C [60]. Later, the same group reported a new type of porous carbon monolith, which was synthesized through a self-assembly approach based on benzoxazine chemistry [61]. The obtained carbon monoliths show crack-free macromorphology, well-defined multilength-scale pore structures, a nitrogen-containing framework, and high mechanical strength (Fig. 2.12).

With such designed structure, the carbon monoliths show outstanding CO_2 capture and separation capacities, high selectivity, and facile regeneration at room temperature. At ~1 bar, the equilibrium capacities of the monoliths are in the range of 3.3–4.9 mmol g^{-1} at 0 °C and of 2.6–3.3 mmol g^{-1} at 25 °C, while the dynamic capacities are in the range of 2.7–4.1 wt% at 25 °C using 14 % (v/v) CO_2 in N_2 (Fig. 2.13). The carbon monoliths exhibit high selectivity for the capture of CO_2 over N_2 from a CO_2/N_2 mixture, with a separation factor ranging from 13 to 28. Meanwhile, they undergo a facile CO_2 release in argon stream at 25 °C, indicating a good regeneration capacity.

Due to the high precision in pore engineering by nanocasting pathway and the great variety of micelle nanostructures deriving from soft templating, many researchers try to combine both techniques into an interdependent and interactive module with the aim of achieving porous carbons with controlled pore structure in a cost-effective manner. Wang et al. [62] prepared 3D ordered macro-/mesoporous porous carbons by using colloidal crystals and surfactants as dual templates through a gas-phase process. In a vapor-phase infiltration, the wall thickness and

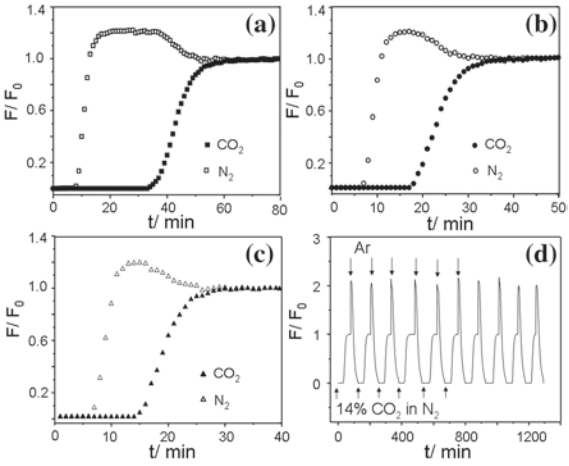

Fig. 2.13 **a–c** Breakthrough curves, a 14 % mixture of CO_2 in N_2 is fed into a bed of HCM-DAH-1, HCM-DAH-1-900-1, and HCM-DAH-1-900-3, respectively. **d** Recycle runs of CO_2 adsorption–desorption on HCM-DAH-1 at 25 °C, using a stream of 14 % (v/v) CO_2 in N_2, followed a regeneration by Ar flow. Reprinted with the permission from Ref. [61]. Copyright 2011 American Chemical Society

window sizes of the carbons are controllable through the variation in the infiltration time. Hierarchical ordered macro-/mesoporous carbon was prepared by dual templating with a hard template (silica colloidal crystals) and a soft template (Pluronic F127), using phenol–formaldehyde precursors dissolved in ethanol [63]. Zhao's group reported a mass preparation of hierarchical carbon–silica composite monoliths with ordered mesopores by using polyurethane (PU) foam as a sacrificial scaffold. The macroporous PU foam provides a large, 3D, interconnecting interface for evaporation-induced self-assembly (EISA) of the coated phenolic resin–silica block copolymer composites, thus endowing composite monoliths with a diversity of macroporous architectures [64]. Recently, the same group reported a direct synthesis of transparent ordered mesostructured resin–silica composite monoliths with uniform rectangular shape through the EISA process by copolymerization of tetraethyl orthosilicate and resol in the presence of triblock copolymer Pluronic F127 as a template [65]. The key factor of this synthesis is the good interoperability and compatibility of the plastic organic resin polymers and the rigid silica skeleton. As a result, multiple choices of the products (ordered mesoporous carbon or silica monoliths with integrated macroscopic morphologies similar to the original composite monoliths) can be realized by either removal of silica in HF solution or elimination of carbon by simple combustion.

To date, the hydrogen-bonding interactions have been extensively explored as the self-assembly driving force between block copolymer surfactants and carbon precursors. As viewed from the current research, the success of hydrogen-bonding induced self-assembly is only in a small mesopore range (3–10 nm). The groundbreaking achievements in achieving well-ordered porosity in either micropore scale (<2 nm) or larger mesopore range (10–50 nm) are still grand challenge. Moreover, the common features of most current syntheses are that they usually take a day, or even longer, and use inorganic catalysts (HCl or NaOH) for the polymerization and self-assembly. Hence, to explore new polymerization systems (new carbon precursors, organic catalysts) that are more time-effective is an exciting research area. In

addition, hierarchical structured monolithic carbons with multimodal porosity would be more suitable for application in gas capture and separation. More desirably, the effluences of multilength-scale pores on the sorption kinetics and storage capability should be figured out by experimental and computational works.

2.4.2.2 Films

Besides the investigation of monolithic carbons with well-ordered mesoporosity as CO_2 sorbents, the synthesis of ordered mesoporous carbon films for CO_2 capture (membrane gas separation) also attracts much interest. Noticeably, highly ordered mesoporous carbon with cubic *Im3m* symmetry has been synthesized successfully via a direct carbonization of self-assembled F108 ($EO_{132}PO_{50}EO_{132}$) and RF composites obtained in a basic medium of non-aqueous solution [66]. Dai et al. [49] demonstrated a stepwise self-assembly approach to the preparation of large-scale, highly ordered nanoporous carbon films (Fig. 2.14).

The synthesis of well-defined porous carbon films involves four steps: (1) monomer–block copolymer film casting, (2) structure refining through solvent annealing, (3) polymerization of the carbon precursor, and (4) carbonization. Zhao et al. [67] reported the fabrication of free-standing mesoporous carbon thin films with highly ordered pore architecture via a simple coating-etching method. The mesoporous carbon films were first synthesized by coating a resol precursors/Pluronic copolymer solution on a pre-oxidized silicon wafer, forming highly ordered polymeric mesostructures based on organic–organic self-assembly, followed by carbonizing at 600 °C and finally etching of the native oxide layer between the carbon film and the silicon substrate. Mild reacting conditions and wide composition ranges are the obvious advantages of the method over the techniques previously reported [51, 68, 69].

Based on mesoporous RF-derived carbon films, Yoshimune et al. [70] investigated the permeation properties of different gases, including H_2, He, N_2, CF_4, and condensable gases of CO_2 and CH_4. As expected, these membranes exhibited relatively high permeances due to their well-developed mesoporous structure. By comparing permeances of the six gases on the RF carbon films at 303 K, the authors found that the gas permeances exhibited a sublinear dependence on the inverse square of the molecular weights, which are predominantly governed by the Knudsen mechanism. Interestingly, the permeances of condensable gases of CO_2 and CH_4 were accelerated. This is because the RF carbon films have both mesopores and a small number of micropores, and the enhanced permeance is attributed to the strong adsorption of condensable gases in the narrower micropores due to the surface diffusion mechanism. However, the effect of molecular sieving mechanism, which allows smaller gas molecules such as those of He to diffuse faster than larger gas molecules such as those of CF_4, is negligible since the gas permeances of the RF carbon membranes are independent of the kinetic diameter of the permeating molecules. Consequently, the transport mechanism of these membranes is mainly governed by Knudsen diffusion, and the existence of a small number of micropores might have induced the surface diffusion.

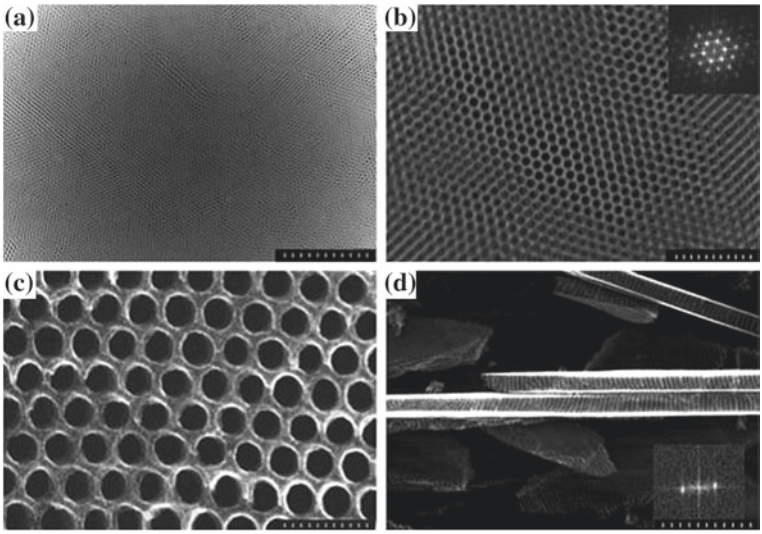

Fig. 2.14 Electron microscopy images of the carbon film. **a** Z-contrast image of the large-scale homogeneous carbon film in a 4 × 3 mm area. The scale bar is 1 mm. **b** Z-contrast image showing details of the highly ordered carbon structure. The scale bar is 300 nm. **c** HR-SEM image of the surface of the carbon film with uniform hexagonal pore array. The pore size is 33.7 ± 2.5 nm, and the wall thickness is 9.0 ± 1.1 nm. The scale bar is 100 nm. **d** SEM image of the film cross section, which exhibits all parallel straight channels perpendicular to the film surface. The scale bar is 100 nm. Reproduced from Ref. [49] by permission of John Wiley & Sons Ltd

Very recently, Hao et al. [71] report a wet-chemistry synthesis of a new type of porous carbon nanosheets whose thickness can be precisely controlled over the nanometer length scale. This feature is distinct from conventional porous carbons that are composed of micron-sized or larger skeletons, and whose structure is less controlled. Smartly, the synthesis uses graphene oxides (GO) as the shape-directing agent and asparagine as bridging molecules that connect the GO and in situ grown polymers by electrostatic interaction between the molecules. The assembly of the nanosheets can produce macroscopic structures, i.e., hierarchical porous carbon monoliths which have a mechanical strength up to 28.9 MPa, the highest reported for the analogs. The synthesis provides precise control of porous carbons over both microscopic and macroscopic structures at the same time. In all syntheses, the graphene content used was in the range 0.5~2.6 wt%, which is significantly lower than that of common surfactants used in the synthesis of porous materials. This indicates the strong shape-directing function of GO. In addition, the overall thickness of the nanosheets can be tuned from 20 to 200 nm (Fig. 2.15) according to a fitted linear correlation between the carbon precursor/GO mass ratio and the coating thickness.

The porous carbon nanosheets show impressive CO_2 adsorption capacity under equilibrium, good separation ability of CO_2 from N_2 under dynamic conditions, and easy regeneration. The highest CO_2 adsorption capacities can reach 5.67 and

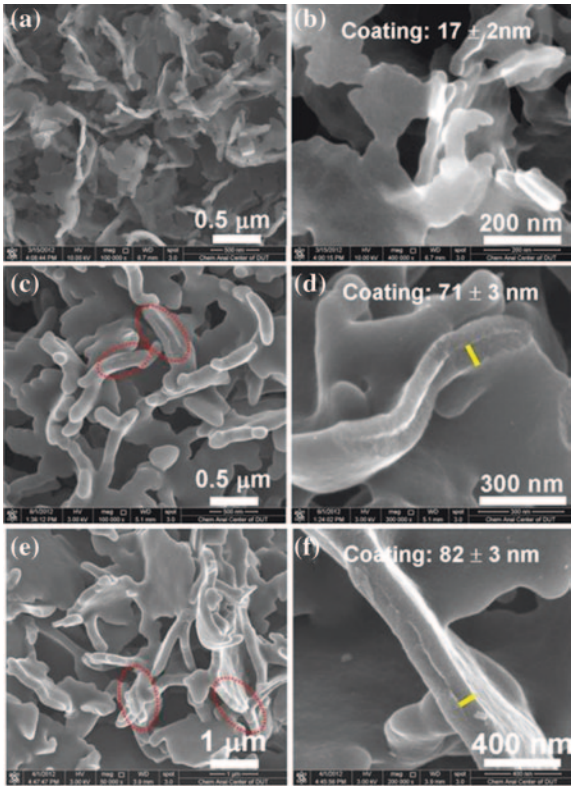

Fig. 2.15 FE-SEM images with low and high magnification of the obtained porous carbon nanosheets with different thickness: **a**, **b** PCN-17, **c**, **d** PCN-71, **e**, **f** PCN-82. The *marked coating* thickness on the *top* of **b**, **d**, **f** is the average thickness based on the measurements. Reproduced from Ref. [71] by permission of The Royal Society of Chemistry

3.54 CO_2 molecules per nm^3 pore volume and per nm^2 surface area at 25 °C and ~1 bar (Fig. 2.16). The probable reason is that the interaction of PCNs samples with CO_2 molecules is strong due to (a) the large amount of microporosity with pore size of ca. 8 Å and (b) the polar surface caused by the residual heteroatom-containing (e.g., O, N) species. These dynamic data provide clear evidence that PCN-17 is extremely selective for adsorbing CO_2 over N_2, which represents a significant step forward in rationally designing a material for dilute CO_2 separation in humid conditions. These values are ideally consistent with the pure CO_2 adsorption data at partial pressures of 0.14, 0.09 and 0.04 bar, indicating its extraordinary moisture resistance. The cycling experiments using $CO_2/H_2O/N_2$ of 4/3/93 v% also verified the selective and reversible CO_2 adsorption capacity of PCN-17 (Fig. 2.16e). A sample saturated with CO_2 was subjected to an Ar purge flow of 15 mL min^{-1} at 50 °C. After approximately 30 min, no CO_2 was detected in the effluent. Successive regenerations reveal that the sample retains more than 97 % of its intrinsic capacity after such mild regeneration (Fig. 2.16f). The 3 % loss of CO_2 capacity may be due to the strongly adsorbed CO_2 on highly active sites. This can be explained by the high Q_{st} at the ultra-low CO_2 uptake. As the regeneration temperature increases to 100 °C, the residual CO_2 (ca. 3 %) can also be recovered.

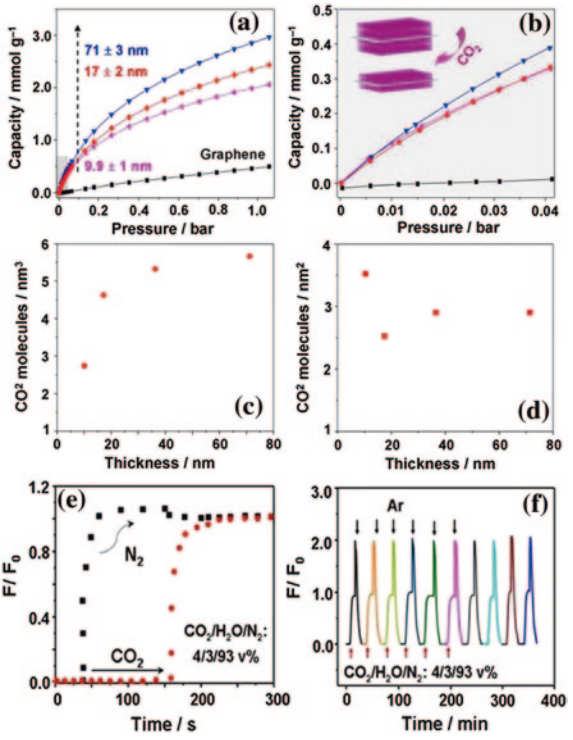

Fig. 2.16 CO_2 adsorption evaluation of the PCNs. **a**, **b** CO_2 adsorption isotherms for high and low CO_2 partial pressures at 25 °C, where the *solid line* represents a Toth model fit to the CO_2 isotherms. **c** The number of CO_2 molecules adsorbed per nm^3 pore volume and **d** per nm^2 surface area for PCNs with different thickness. **e**, **f** CO_2 separation evaluation of PCN-17 in dynamic breakthrough tests. **e** Breakthrough *curves* and **f** cycling of CO_2 separation from a stream of $CO_2/H_2O/N_2$ of 4/3/93 v% at 25 °C, following a regeneration by an Ar purge at 50 °C. Reproduced from Ref. [71] by permission of The Royal Society of Chemistry

2.4.2.3 Spheres

The synthesis of porous carbon nanospheres for CO_2 capture is another important topic due to their combined features such as shortened dimensions, increased surface area, easy surface or bulk functionalization. Generally, CS include solid spheres and hollow spheres, which can be prepared through either self-assembly method or templating way [72, 73]. For example, Liu et al. [74] developed a methodology to synthesize monodisperse RF resin polymer colloidal spheres and their carbonaceous analogs through a modified Stöber method. The key to the successful synthesis is using ammonia in the reaction system; its role, they consider, lies in not only accelerating the polymerization of RF, but also supplying the positive charges that adhere to the outer surface of spheres to prevent particle aggregation. The particle size of the RF resin colloidal spheres obtained can be finely tuned by changing the ratio of alcohol/water, the amounts of ammonia and RF precursor, using alcohols with short alkyl chains, or introducing the triblock copolymer surfactant.

Following the same synthesis principle, Jaroniec et al. reported the preparation of a series of CS by carbonization of phenolic resin spheres via the modified Stöber method. As shown in Fig. 2.17, all samples show spherical morphology with the average diameter of 570, 420, 370, and 200 nm for as-synthesized CS-6, CS-6-CD-4, CS-6-CD-8, CS-6-CD-12 carbon spheres, respectively. The particle

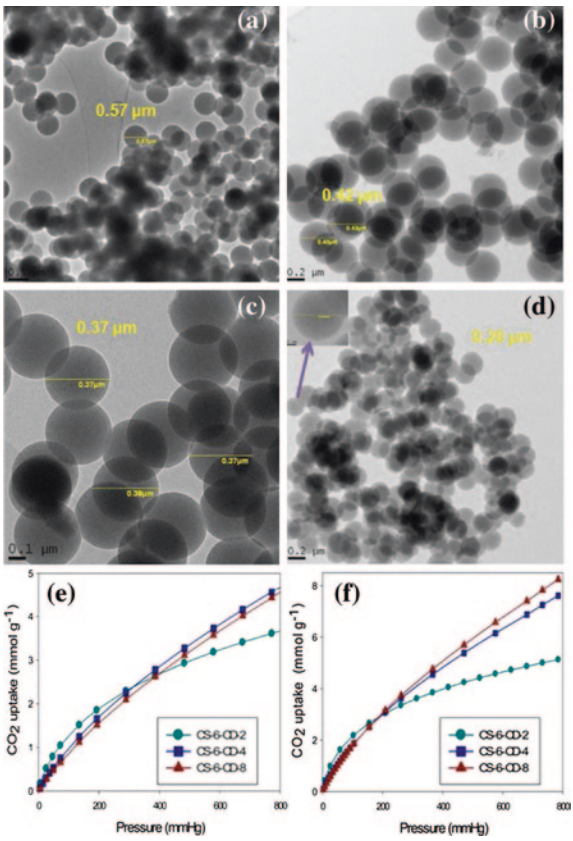

Fig. 2.17 TEM images of CS-6 (**a**), CS-6-CD-4 (**b**), CS-6-CD-8 (**c**), and CS-6-CD-12 (**d**). CO_2 adsorption isotherms for CS-6-CD-t measured at 25 °C (**e**) and 0 °C (**f**). Reprinted with the permission from Ref. [75]. Copyright 2013 American Chemical Society

size is decreasing with increasing activation time, indicating deterioration of the outer surface of CS with activation time. The obtained activated CS having high surface area (from 730 to 2,930 $m^2\ g^{-1}$), narrow micropores (<1 nm), and, importantly, high volume of these micropores (from 0.28 to 1.12 $cm^3\ g^{-1}$) are obtained by CO_2 activation of the aforementioned CS. The remarkably high CO_2 adsorption capacities, 4.55 and 8.05 mmol g^{-1}, are measured on these carbon nanospheres at 1 bar and two temperatures, 25 and 0 °C, respectively [75].

The CO_2 adsorption capacity of CS depends not only on their textural characteristics, but also on the surface chemistry, which can be modified with different methodologies. For example, nitrogen-doped phenolic resin-based CS were prepared by a slightly modified Stöber method using ammonia as nitrogen source. The as-synthesized phenolic resin spheres and the CS obtained by carbonization of polymer spheres at 600 °C showed spherical morphology with the average diameter of 600 and 550 nm, respectively. A direct KOH activation of polymeric spheres gave carbons with small micropores (<0.8 nm) and large specific surface area (2,400 $m^2\ g^{-1}$), which are able to adsorb an unprecedented amount of CO_2 (up to 8.9 mmol g^{-1}) at 0 °C and ambient pressure [76].

Later on, the same group also reported a series of cysteine-stabilized phenolic resin-based polymer and CS prepared by the modified Stöber method [77]. They believe cysteine plays a very important role in the formation of such nanospheres, acting as a particle stabilizer and a source of heteroatoms (nitrogen and sulfur) that can be introduced into these spheres. The diameter of these spheres can be tuned in the range of 70–610 nm by adjusting the cysteine amount and reaction temperature. Since polymer spheres obtained in the presence of cysteine contain sulfur and nitrogen heteroatoms, they are promising in CO_2 capture.

For the research regarding CS, another important trend is to prepare monodisperse, uniform, and colloidal spheres, which can serve as model carbons for fundamental analysis in many applications including CO_2 capture. For example, Xu's group has created a novel and general method to prepare monodisperse carbon nanospheres with a regular round ball-like shape [73, 78]. In their synthesis, three steps are involved: (1) synthesize monodisperse polystyrene spheres by soap-free emulsion polymerization; (2) increase the surface cross-linking degree of polystyrene spheres via Friedel Crafts alkylation as a post-cross-linking reaction; (3) carbonize the reaction product. By adjusting the post-cross-linking reaction time, the size of hollow core can be finely tuned. This is a novel method in the field of fabrication of CS.

Furthermore, it has been known that monodisperse colloidal spheres have the ability to self-assemble into three-dimensional periodic colloidal crystals, only when their size distributions are less than 5 % [79]. That is a particular challenge to establish a new and facile synthesis strategy toward truly monodispersed carbon nanospheres [80]. Wang et al. [81] have established a new strategy of synthesis of highly uniform carbon nanospheres with precisely tailored sizes and high monodispersity on the basis of the benzoxazine chemistry.

2.4.3 Hard-Templated Porous Carbons

Nanocasting is a process in which a mold (may be called as hard template, scaffold) over nanometer scale is filled with a precursor, and after processing, the initial mold is afterward removed [82–87]. In this way, the space once occupied by the host mold is thus transferred into pores of the final carbon products, and the carbon in the original template pores is released as a continuous carbon framework. Nanocasting usually involves the following steps: (1) preparation of a porous template with controlled porosity; (2) introduction of a suitable carbon precursor into the template pores through techniques such as wet impregnation, CVD, or their combination; (3) polymerization and carbonization of the carbon precursor to generate an organic–inorganic composite; and (4) removal of the inorganic template. In the past decades, nanocasting pathway has been demonstrated as a controllable method in preparing carbon monoliths with tailorable pore size over several length scales. The keys rely on preparing a template with accessible porosity and a thermal stable carbon precursor such as phenolic resin, sucrose, furfuryl alcohol (FA), acrylonitrile, acetonitrile, and mesophase pitch. In the following part, we discuss the detailed synthesis principle based on several representative examples.

2.4.3.1 Porous Carbons Replicated from Porous Silica

Porous carbons replicated from porous silica are extensively investigated. For example, Lindén and coworkers prepared hierarchical porous monolithic carbon containing wormholelike mesopores and macropores [88–90]. In a similar way, Shi et al. [91] prepared a novel porous carbon with co-continuous structure and trimodal pores using a hierarchical silica monolith as the template. Hu et al. [92] synthesized hierarchically porous carbons with a relatively higher graphite-like ordered carbon structure by using meso-/macroporous silica as a template and using mesophase pitch as a precursor. Yin' group also reported a preparation of mesoporous nitrogen-doped carbon (N-MC) with highly ordered two-dimensional hexagonal structures using diaminobenzene (DAB) as carbon and nitrogen sources, ammonium peroxydisulfate (APDS) as an oxidant, and SBA-15 as a hard template [93]. By adjusting the synthesis temperatures in a range of 70–100 °C, the pore diameter of the as-made materials can be tuned from 3.4 to 4.2 nm, while the specific surface area of the N-MC with a nitrogen content of 26.5 wt% can be tuned from 281.8 to 535.2 $m^2\ g^{-1}$. The C/N molar ratio of the samples can be tuned in a range of 3.25–3.65 by adjusting the mole ratio of DAB/APDS precursors at a synthesis temperature of 80 °C, while the pore diameter of the N-MC can be tuned in a range of 4.1–3.7 nm.

The above nanocasting method was far more successful, but the multisteps and long synthesis period it involved are impressive. To simplify the tedious procedures, researchers made massive efforts. Han and coworkers developed a one-step nanocasting technique to synthesize micro-/mesoporous carbon monoliths with very high BET surface area (ca. 1,970 $m^2\ g^{-1}$) and ca. 2 nm mesopores by the cocondensation of β-cyclodextrin with tetramethylorthosilicate [94].

Carbon nitride (CN) is a well-known and fascinating material that has attracted worldwide attention because the incorporation of nitrogen atoms in the carbon nanostructure can improve the mechanical properties and surface chemistry. As a result, increasing efforts have been recently devoted to the synthesis of CN. Vinu et al. prepared two-dimensional mesoporous carbon nitride (MCN) with tunable pore diameters using SBA-15 materials with different pore diameters as templates through a simple polymerization reaction between ethylenediamine (EDA) and carbon tetrachloride (CTC) by a nano hard-templating approach [95]. HRTEM was used to further examine the structural order and morphology of the mesoporous CN materials with different pore diameters. The pore diameter of the MCN materials can be easily tuned from 4.2 to 6.4 nm without affecting their structural order. The carbon-to-nitrogen ratio of the MCN decreases from 4.3 to 3.3 with increasing weight ratio of EDA to CTC from 0.3 to 0.9. The optimum EDA-to-CTC weight ratio required for fabricating the well-ordered MCN materials with excellent textural parameters and high nitrogen content is around 0.45. The specific surface area and the specific pore volume of MCN materials can be adjusted ranging between 505 and 830 $m^2\ g^{-1}$ and 0.55–1.25 $cm^3\ g^{-1}$.

In a similar way, Zhao's group reported the preparation of porous CN spheres with partially crystalline frameworks via a nanocasting approach by using spherical mesoporous cellular silica foams (MCFs) as a hard template, and EDA and

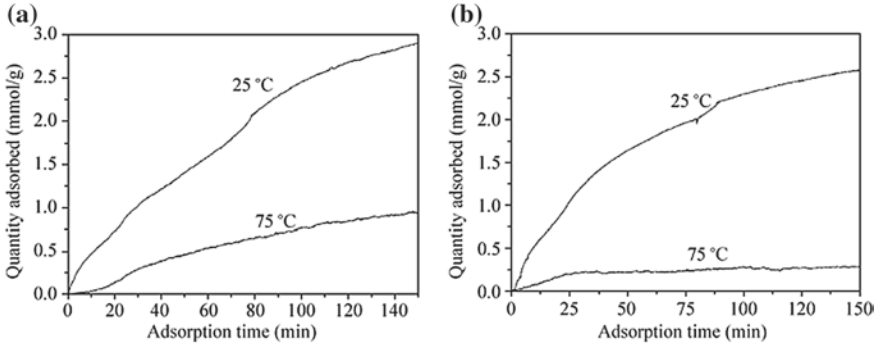

Fig. 2.18 CO_2 capture capacities of **a** the mesoporous CN materials and **b** the pristine CS at 25 and 75 °C. Reprinted from Ref. [96], with kind permission from Springer Science+Business Media

CTC as precursors. The elemental analyses show that the material has high nitrogen content (17.8 wt%) with nitrogen-containing groups and abundant basic sites. The obtained CN spheres have mesostructure with small and large mesopores with pore diameters centered at ca. 4.0 and 43 nm, respectively, a relatively high BET surface area of ~550 $m^2\ g^{-1}$, and a pore volume of 0.90 $cm^3\ g^{-1}$. The adsorption isotherms of the mesoporous CN spheres (Fig. 2.18a) show that after adsorption for 150 min, CO_2 uptake reaches 2.90 mmol g^{-1} at 25 °C. When the temperature was increased to 75 °C, the uptake greatly decreased to 0.97 mmol g^{-1}. The CO_2 uptake (2.50 mmol g^{-1}) of the pristine carbon material (Fig. 2.18b) was similar to that of the mesoporous CN sample at 25 °C. However, when the temperature was increased to 75 °C, its CO_2 uptake decreased dramatically to 0.30 mmol g^{-1}, which is much lower than the corresponding value of the mesoporous CN spheres, suggesting that there is a weak interaction between the carbon pore walls and CO_2 molecules [96].

2.4.3.2 Porous Carbons Replicated from Crystalline Microporous Materials

As shown in Fig. 2.19, the nanocasting pathway is also powerful to produce nanoporous carbons with remarkably high surface areas (up to 4,000 $m^2\ g^{-1}$) and precisely controlled microporous structures (0.5–1.5 nm) that are well suitable for CO_2 capture [97]. The efforts to construct such molecular-sieve-type porous carbon using well-crystalline zeolite or MOFs-related materials (ZIFs, MOCPs) as sacrificial templates still continue.

Banerjee et al. [98] reported a synthesis and gas adsorption properties of porous carbons synthesized by a nanocasting method at 1,000 °C, in which isoreticular zeolitic imidazolate frameworks (IRZIFs) acts as the template and FA as carbon source. Similarly, Deng et al. [99] synthesized a series of porous carbons from non-porous metal–organic coordination polymers (MOCPs), using in situ polymerized phenol resin as the carbon precursor. The textural properties of highly

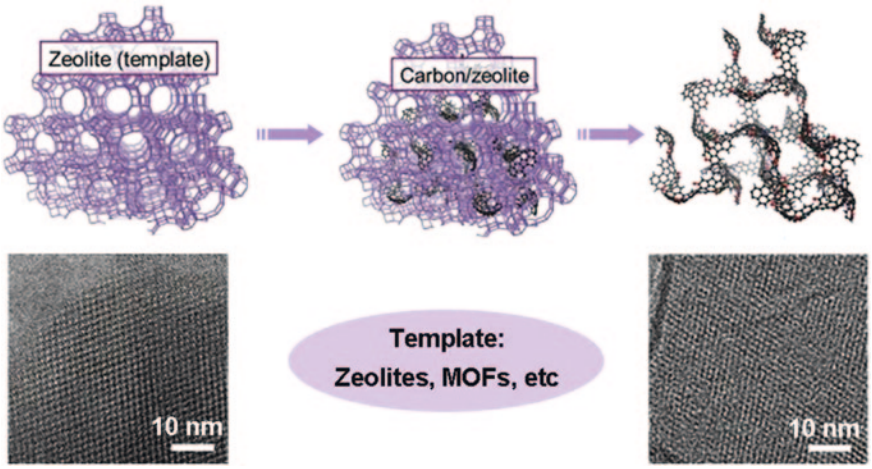

Fig. 2.19 Synthesis of molecular sieve carbon (MSC) through nanocasting pathway: The sacrificial templates include the crystalline zeolites and MOFs. Reproduced from Ref. [97] by permission of John Wiley & Sons Ltd

microporous ZIF-templated carbons derived from commercially available ZIFs (Basolite Z1200) can be further improved via mild chemical activation, as demonstrated by Almasoudi and Mokaya [100].

Moving one-step forward, the direct transformation of MOFs-related materials (PCPs, ZIFs, PAFs, etc.) to porous carbons with nanopores of a precise and uniform size has been achieved through simple carbonization at elaborate temperature. This synthesis strategy for nanoporous carbons is a burgeoning new area of research, which will further broaden the library of MSCs. Yamauchi et al. [101] have pioneered the synthesis of a novel nanoporous carbon with highly developed porosity (surface area of 5,500 $m^2\ g^{-1}$ and pore volume of 4.3 $cm^3\ g^{-1}$) by a direct carbonization of Al-PCPs. Porous carbons with hierarchical pore structures could also be achieved by direct carbonization of the selected IRMOFs (IRMOF-1, IRMOF-3, and IRMOF-8), indicating the tunable pore characteristics of MOFs-derived nanoporous carbons [102]. Ariga et al. [103] reported a nanoporous carbon with high surface areas (up to 1,110 $m^2\ g^{-1}$), and narrow pore size distributions that are close to its parent ZIF-8.

A family of nanoporous carbons has also been prepared by thermal decomposition of guest-free MOFs (even non-porous MOFs) by Kim and colleagues [104]. They found that the porosity of the carbon materials depends linearly on the Zn/C ratio of MOFs precursors, which allow a precise control of the porosity of the carbon materials in a predictable manner.

Through a simple pyrolysis of crystalline polymer (PAF-1), Qiu et al. [105] have prepared a series of nanoporous carbons having high surface areas and narrow micropore size distributions. The carbonized (at 450 °C) sample PAF-1-450 showed very excellent adsorption capacities (4.5 mmol g^{-1}) for CO_2 than that of original PAF-1 at ambient conditions (Fig. 2.20). These aforementioned works exemplify a

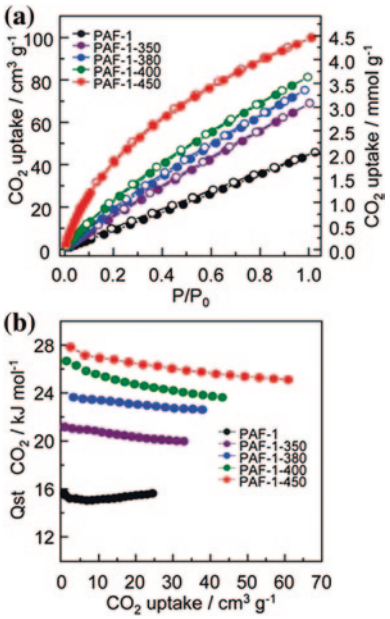

Fig. 2.20 **a** CO_2 adsorption (*solid symbols*) and desorption (*open symbols*) isotherms of PAF-1 and carbonized samples at 273 K; **b** Q_{st} CO_2 of PAF-1 and carbonized samples as a function of the amount of CO_2 adsorbed. Reproduced from Ref. [105] by permission of The Royal Society of Chemistry

striking indication that the facile and one-step pathway replicated from crystalline microporous materials is highly efficient toward highly nanoporous carbons.

2.4.3.3 Porous Carbons Replicated from Colloidal Crystals

Colloidal crystals are the self-assembly periodic structures consisting of close-packed uniform particles. In most cases, replication of the colloidal crystals (colloidal silica/polymer spheres) will lead to a high degree of periodicity in three dimensions. Subsequent removal of the crystal templates results in a replica with 3D-ordered macroporous (3DOM) structures. The groups of Stein, Velev, and Lenhoff have independently achieved many great results in the field of colloidal crystal and their related areas. Here, we only discuss a small aspect where the templating of colloidal crystal is used as an effective path to get porous carbons with highly ordered macroporosity. For example, Lee et al. [106] synthesized 3DOM carbons via a RF sol-gel process using poly(methyl methacrylate) colloidal crystal templates. Similarly, Adelhelm et al. [107] also synthesized a hierarchical meso- and macroporous carbon using mesophase pitch as precursors and PS or PMMA as templates through spinodal decomposition.

By carbonization of a thin layer of phenolic resin on the suitable templates, Gierszal et al. [108] reported the synthesis of one kind of uniform carbon film with large pore volumes (6 $cm^3\ g^{-1}$ for 24 nm silica colloids), uniform pore sizes, and controlled thickness. This synthetic route involves the formation of a uniform polymeric film on the silica pore walls of silica colloidal crystals or colloidal aggregates and its carbonization and template removal. After proper pre-treatment of the silica

template and under controlled experimental conditions, the mixture of resorcinol and crotonaldehyde copolymerizes on the silica surface and form a uniform film. Recently, Zhang and coworkers presented a one-pot method to synthesize hierarchically bimodal-ordered porous carbons with interconnected macropores and mesopores, via in situ self-assembly of colloidal polymer (280, 370, and 475 nm) and silica spheres (50 nm) using sucrose as the carbon source. Compared with the classical nanocasting procedure, this approach is veritably simple; neither pre-synthesis of crystal templates nor additional infiltration is needed, and the self-assembly of polymer spheres into the crystal template and the infiltration are finished simultaneously in the same system [109]. Similarly, a hierarchically porous carbon with multimodal (macropore and mesopore) porosity have also been prepared by using dual-template (PS/colloidal silica and PMMA/colloidal silica), where PS (or PMMA) is used for creating 3D-ordered macropores, colloidal silica is responsible for creating spherical mesopores [110, 111]. The unique hierarchical structures of 3DOM carbons, i.e., the open larger mesopores located in the ordered macropores may enhance the kinetics greatly when used as CO_2 sorbents.

2.4.3.4 Porous Carbons Replicated from MgO nanoparticles

Park et al. [112] reported a series of porous carbons with well-developed pore structures, which were directly prepared from a weak acid cation exchange resin (CER) by the carbonization of a mixture with Mg acetate in different ratios (Fig. 2.21). By dissolving the MgO template, the porous carbons exhibited high specific surface areas (326–1,276 $m^2\ g^{-1}$) and high pore volumes (0.258–0.687 $cm^3\ g^{-1}$). The CO_2 adsorption capacities of the porous carbons were enhanced to 164.4 mg g^{-1} at 1 bar and 1,045 mg g^{-1} at 30 bar by increasing the Mg-acetate-to-CER ratio. This result indicates that CER is one of the desirable carbon precursors for producing the porous structure, as well as improving the CO_2 adsorption capacities of the carbon species.

Recently, Jang's group reported a time-saving synthesis toward ordered mesoporous carbon supported MgO (Mg-OMC) materials, which were fabricated by the carbonization of sulfuric acid-treated silica/triblock copolymer/sucrose/$Mg(NO_3)_2$ composites. In the current approach, triblock copolymer P123 and sucrose were employed as both structure-directing agents for the self-assembly of rice husk ash silica solution and carbon precursor. Sulfuric acid was used to cross-link P123 and sucrose in the as-synthesized composites in order to improve the carbon yield. The CO_2 adsorption capacity of Mg-OMC-1 was observed to be 92 mg g^{-1}, which is comparable with that of the well-established CO_2 sorbents [113].

Przepiórski et al. reported the competitive uptake of SO_2 and CO_2 on the porous carbon materials containing CaO and MgO, prepared by carbonization of poly(ethylene terephthalate) mixed with a natural dolomite. The as-prepared porous carbon was examined as a sorbent for simultaneous removal of CO_2 and SO_2 from air in dry conditions and in a presence of humidity, at temperatures ranging from 20 to 70 °C. The attained results clearly confirmed the crucial effect of water on the amounts of gases removed from air streams and the removal mechanisms. The

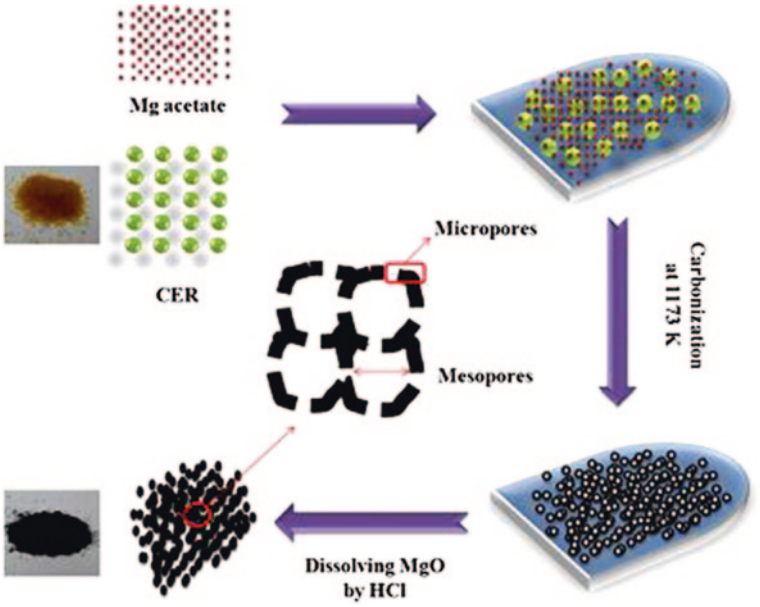

Fig. 2.21 Schematic representation of the preparation of MgO-templated nanoporous carbons. Reprinted from Ref. [112]. Copyright 2012, with permission from Elsevier

breakthrough curves registered clearly revealed the overshoot in concentration of the gas during the first minutes of removal tests (Fig. 2.22) [114].

Recently, Park et al. reported the preparation of nanoporous (styrene-divinylbenzene)-based ion exchange resin-based carbons (MPCs) by MgO-templating synthesis and KOH activation. MPCs were prepared from a (styrene-divinylbenzene)-based ion exchange resin by the carbonization of a mixture with Mg gluconate at 900 °C. And then, the prepared MPCs were treated with KOH at KOH/MPCs ratios ranging from 0.5 to 4 at 800 °C. Low KOH/MPCs ratios (KOH/MPCs ratio = 1, MCK-1) tended to favor the formation of micropores, whereas higher KOH/MPCs (KOH/MPCs ratio = 4, MCK-4) led to the formation of mesopores. The treated MPCs with a KOH/MPCs ratio = 1 exhibited the best CO_2 adsorption value of 266 mg g^{-1} at 1 bar. However, the treated MPCs with a KOH/MPCs ratio of 3 (MCK-3) exhibited the best CO_2 adsorption value of 1,385 mg g^{-1} at 30 bar. This result indicated that the CO_2 adsorption capacity of nanoporous carbons is attributed to the mesopore volume fraction at higher pressure [115].

2.4.4 Porous Carbon-Based Composites

Post-modification is a versatile method for the preparation of advanced carbons with powerful functions through processes such as CVD [116, 117], impregnation [118–120], and metal transfer reactions [121].

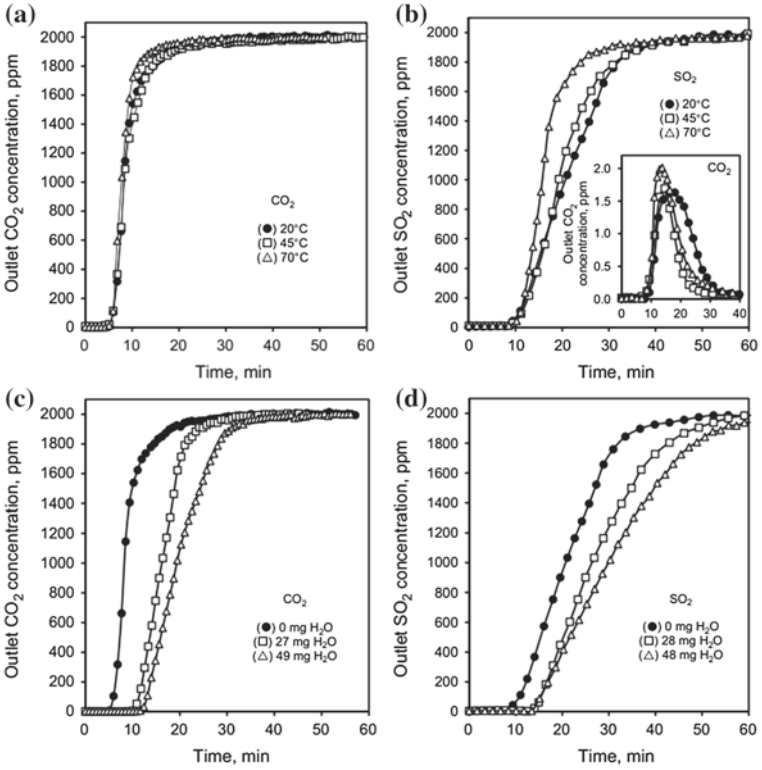

Fig. 2.22 Breakthrough curves for MgO-/CaO-loaded carbon sorbent exposed to air contaminated with CO_2 or SO_2 at different experimental temperatures: 20, 40, 70 °C (**a** and **b**) and at 20 °C after pre-humidification conducted for different times (**c** and **d**). Reprinted from Ref. [114]. Copyright 2013, with permission from Elsevier

García-Martínez et al. [122] reported a solvent-free, liquid-phase synthesis of self-assembled carbon foams, which can be prepared in variable shapes and morphologies without the need of any binders. Long et al. [123] prepared carbon aerogels by sol-gel polymerization of phenol, melamine and formaldehyde, followed by subsequent carbonization process. The as-prepared samples showed 3D mesoporosity and large pore volume, which allow easy diffusion of reactants and products, and served as the reservoir for the guest molecules. Using similar procedure, Nielsen et al. [124] prepared $2LiBH_4$-MgH_2/carbon aerogel systems as hydrogen storage materials through the nanoconfined chemistry. In this designed composite, $LiBH_4$ and MgH_2 nanoparticles were embedded in a nanoporous carbon aerogel scaffold with pore size (D_{max}) of 21 nm and reacted to form MgB_2 during release of hydrogen.

Besides post-modification, a direct copolymerization is suitable not only for introduction of molecular functional groups to the carbon products, but also allows well dispersion of nanoparticles throughout the carbon framework. Researchers from

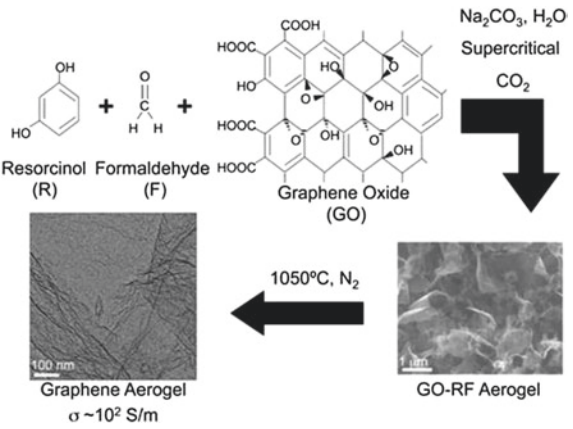

Fig. 2.23 Synthesis procedure for the GO-RF aerogel and graphene aerogel. Reprinted with the permission from Ref. [128]. Copyright 2010 American Chemical Society

Lawrence Livermore National Laboratory have made major advances in the synthesis and functionalization of monolithic carbon aerogels [125, 126]. Recently, they reported TiO_2/C, TiCN/C, ZnO/C composite aerogels by carbothermal reduction in the titania (or ZnO)-coated carbon aerogels. The resulting monoliths consisting of nitrogen-rich titanium carbonitride ($TiC_{1-x}N_x$, $x = 0.90$) nanocrystals or well-crystallized ZnO nanoparticles exhibited surface areas of 1,838 and 1,500 $m^2\ g^{-1}$, respectively. Also, they successfully integrated CNTs or graphene sheets into the sol-gel reaction, leading to the formation of the advanced monolithic carbons with significantly improved mechanical properties [127–129]. This strategy has used the organic RF binder that is reducible concurrently with the GO or CNTs to thus produce carbon cross-links in the graphene or CNTs network which are virtually indistinguishable from those in the graphene sheets or CNTs networks (Fig. 2.23).

Recently, Jin et al. [130] reported a new type of CNT-modified carbon monoliths that were prepared from a commercial phenolic resin mixed with just 1 wt% of CNTs followed by carbonization and physical activation with CO_2. The products possess a hierarchical macro-/microporous structure and superior CO_2 adsorption properties. In particular, they show the top-ranked CO_2 capacity (52 mg CO_2 per g adsorbent at 25 °C and 114 mmHg) under low CO_2 partial pressure, which is of more relevance for flue gas applications. This study demonstrates an effective way to create narrow micropores through structural modification of carbon composites by CNTs.

From an application point of view, the volumetric capacities are even more important than that on a gravimetric basis, due to the limited volume of the gas storage tank. Under this consideration, Qian et al. [131] optimized the structural features of hierarchical porous carbon monolith by incorporating the advantages of MOFs ($Cu_3(BTC)_2$) to maximize the volumetric based CO_2 capture capability (CO_2 capacity in cm^3 per cm^3 adsorbent). The mesoscopic structure of the HCM-$Cu_3(BTC)_2$ composites and the parent materials (HCM and $Cu_3(BTC)_2$) were characterized by SEM. The SEM micrograph (Fig. 2.24) clearly displays that $Cu_3(BTC)_2$ crystallites are born within the macropores of the HCM matrix. The sponge-like skeleton of HCM before and after the MOF growth remains

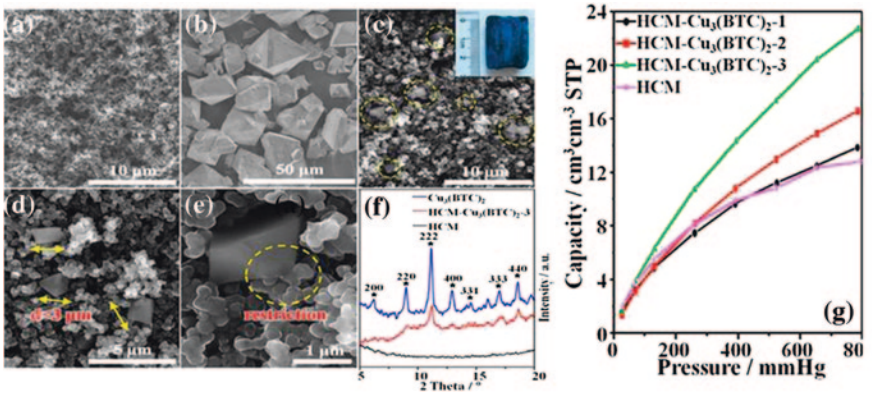

Fig. 2.24 SEM micrographs of HCM (**a**), $Cu_3(BTC)_2$ (**b**), and HCM-$Cu_3(BTC)_2$-3 (**c**–**e**). (**f**) XRD patterns of HCM, $Cu_3(BTC)_2$, and HCM-$Cu_3(BTC)_2$−3. (**g**) CO_2 adsorption isotherms on a volumetric basis. Reprinted with the permission from Ref. [131]. Copyright 2012 American Chemical Society

unchanged. The octahedral $Cu_3(BTC)_2$ crystallites are well dispersed within the HCM matrix. The equilibrium CO_2 adsorption measurements were carried out at 25 °C, and the results (Fig. 2.24) reveal that HCM-$Cu_3(BTC)_2$ composites exhibit an obvious increment in CO_2 adsorption capacity on a volumetric basis compared with the original HCM. The HCM-$Cu_3(BTC)_2$-3 composite with the highest $Cu_3(BTC)_2$ loading can achieve maximum CO_2 uptake of 22.7 cm^3 STP per cm^3 at ~1 bar, which is almost as twice as the uptake of HCM (12.9 cm^3 STP per cm^3) under the same conditions. This result encourages a new principle on a rational design of CO_2 capture material by maximizing the capacity on a volumetric basis.

2.5 Graphitic Porous Carbons for CO_2 Capture

2.5.1 Bulk Crystalline Porous Carbons

Porous carbons obtained through the above-mentioned methods, in most cases, have the amorphous carbon walls, which contain either adventitious micropores or templated open mesopores. Due to the long range randomly arrangement of the primary carbon fragments, the amorphous carbon possesses abundant active sites and displays various kinds of porosity, thus leading to a high surface area. These properties endowed by the amorphous feature combined with the ease of handling render the amorphous carbons to be widely used in many fields such as catalysis, adsorption/separation, hydrogen storage, and desalination.

Besides amorphous carbons, graphitic porous carbons are also widely investigated and may be valuable for figuring out the CO_2 capture behavior due to its

ordering at the atomic scale. Though high-temperature thermal treatments above 2,000 °C can facilitate the transition to graphitization phase, unfortunately, it often results in a partial or total collapse of the pore structures and reduces the accessible surface areas. By employing graphitization catalysts (i.e., Fe or Co salt) [132], one can obtain graphitic porous carbons, in which an additional leaching process is required to remove the final metal oxide derived from the catalyst precursors. Liang et al. [133] reported the synthesis of graphitic carbon column with bimodal pores, which was prepared by pyrolyzing a rod made of a copolymer of a resorcinol/iron(III) complex and formaldehyde in the presence of silica beads through a nanocasting process. Very recently, Dai's group pioneered a "brick-and-mortar" self-assembly approach toward ordered graphitic mesoporous carbon nanocomposites with tunable mesopore sizes below 850 °C without using graphitization catalysts or high-temperature thermal treatments [134]. In this strategy, phenolic resin-based mesoporous carbons act as mortar, while the highly conductive carbon blacks or carbon onions were introduced as bricks that are responsible for the graphitic domains of the pore walls. This breakthrough provides a new approach to the synthesis of porous carbons with high level of graphitization under a facile condition.

2.5.2 2D Nanosheets/Films

The emergence of graphene nanosheet has opened up an exciting new field in the science and technology of two-dimensional nanomaterials [135–137]. Graphite oxide (GO) is a derivative of graphene and consists of oxygen functional groups on their basal planes and edges, so surface modification of GO with amines or amine-containing molecules takes place easily through the corresponding nucleophilic substitution reactions. If polyamines covalently attach to their layers, the residual unreacted amine groups can react with CO_2 and have potential for the removal of CO_2. Under this consideration, Zhao et al. prepared GO–amine composites based on the intercalation reaction of GO with amines, including EDA, diethylenetriamine (DETA), and triethylene tetramine (TETA). Dynamic CO_2 breakthrough test revealed that the aminated GO was an efficient adsorbent for CO_2 capture. For example, the typical sample of GO/EDA showed an adsorption capacity of 53.62 mg g^{-1} sample [138].

Srinivas et al. [136] reported a method to obtain a wide range of highly porous carbon adsorbents through chemical activation of exfoliated graphene oxide precursors with KOH. Through tuning the synthesis, they successfully prepared a series of GO-derived carbons (GODCs) that showed different porous structures (Table 2.2). By comparing porous properties with respect to the gas adsorption capacity of this new class GODCs with a range of other porous solids including ACs and metal–organic frameworks, they believe that the GODCs have a great potential in gas adsorption applications.

Very interestingly, Koenig et al. [139] pioneered one type of interesting graphene membrane-based molecular sieve. In their synthesis method, ultraviolet-induced

Table 2.2 GODCs with synthesis conditions (KOH/exf-GO concentration and activation temperature), yield by weight of precursor exf-GO, the porosity parameters: BET surface area, average pore size, porosity based on a skeleton density of 2 g cm^{-3}, and high-pressure CO_2 and methane adsorption capacities at 20 and 35 bar, respectively, at 300 K

Sample	Yield by weight (%)	BET surface area/m^2 g^{-1}	Total pore volume/cm^3 g^{-1}	Average pore size/nm	Porosity (%)	CO_2 adsorption/ mg mg^{-1}	Methane adsorption/ mg mg^{-1}
GODC4-600	54	916	0.48	1.3	49	0.390	0.096
GODC9-600	36	619	0.36	1.54	42	0.360	0.084
GODC4-700	53	1,096	0.56	1.54	53	0.480	0.119
GODC9-700	28	1,326	1.10	1.85	69	0.555	0.137
GODC4-800	38	1,276	0.72	1.60	59	0.497	0.126
GODC9-800	26	1,704	1.65	2.6	77	0.652	0.163
GODCsol-800	33	1,894	1.60	2.4	76	0.721	0.175
GODCsol-900	10	1,272	0.99	1.86	66	0.525	0.137

Reproduced from Ref. [136] by permission of The Royal Society of Chemistry

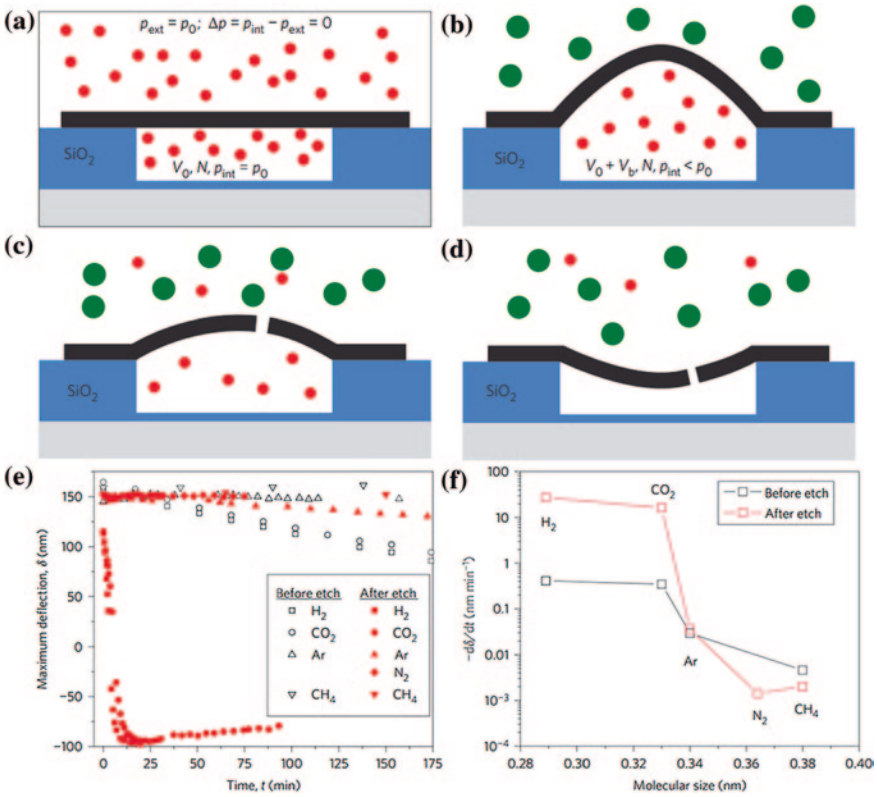

Fig. 2.25 Measuring leak rates in porous graphene membranes. **a** Schematic of a microscopic graphene membrane on a silicon oxide substrate. **b** After removing the graphene membrane from the pressure chamber, the membrane bulges *upwards*. **c** Following etching pore(s) in the graphene membrane bigger than H_2, the H_2 is able to rapidly leak out of the microchamber through the membrane pore(s). **d** Once all the H_2 molecules have leaked out of the microchamber, the membrane will deflect *downwards*. Comparison of leak rates of pristine and porous graphene membranes. **e** Maximum deflection δ versus t before and after etching. **f** Average $-d\delta/dt$ versus molecular size found from the slopes of membrane deflection versus t (in **e**) before and after introducing pores into the same graphene membrane. The connecting lines show the measurements before (*black*) and after (*red*) etching. Reprinted by permission from Macmillan Publishers Ltd.: Ref. [139], Copyright 2012

oxidative etching can create pores in micrometer-sized graphene sheets (Fig. 2.25). A pressurized blister test and mechanical resonance are used to measure the transport of a range of gases (H_2, CO_2, Ar, N_2, CH_4, and SF_6) through the pores. The molecular selectivity of the fabricated porous graphene membrane was demonstrated by measuring the rate of change of δ with time ($-d\delta/dt$) for the same membrane pressurized with a number of different gases. Figure 2.25a shows δ versus t for H_2, CO_2, Ar, and CH_4 before and after etching, and N_2 after etching. At short times, $-d\delta/dt$ is approximately linear. This rate was plotted versus kinetic diameter for all the gases, using

the same membrane/microcavity, before and after etching (Fig. 2.25b). After etching, there is an increase in $-d\delta/dt$ by two orders of magnitude for the H_2 and CO_2 leak rates, whereas those for Ar and CH_4 remain relatively unchanged. This suggests that the etched pores change the transport mechanism for H_2 and CO_2, but leave the transport of Ar and CH_4 nearly unchanged. The experimental results reveal the realization of graphene gas separation membranes by molecular sieving and represent an important step toward the realization of size-selective porous graphene membranes.

Besides graphene sheets tested as CO_2 capture materials, the introduction of other active sites onto graphene sheets for high-performance CO_2 sorbents was also extensively investigated recently [140–142]. For example, PPy functionalized graphene sheets are employed to fabricate N-doped porous carbons via chemical activation [143]. This type of material shows selective adsorption of CO_2 (4.3 mmol g^{-1}) over N_2 (0.27 mmol g^{-1}) at 25 °C. Similarly, the highest CO_2 uptake (75 mmol g^{-1}) at 11 bar and 25 °C over polyaniline–graphene nanocomposites were reported by Mishra and Ramaprabhu [144].

2.5.3 1D Carbon Nanotubes/Fibers/Ribbons/Scrolls

Another familiar carbon nanostructure is carbon nanotube. Since the first synthesis of carbon nanotubes (CNTs) via arcing between graphite-like electrodes by Iijima in 1991 [145], 1D carbon materials have been extensively researched, due to their outstanding properties such as excellent chemical and thermal stability, high surface area, and potential applications in electronics, adsorption, and catalysis. So far, CVD [146, 147] and the electrospinning technique [148] have been widely used in the production of 1D carbon materials. One of their potential applications is as sorbents for CO_2 capture due to their shortened size, easy functionalization, and/or integration with foreign active species for selective CO_2 recognition [149–153].

For example, Dillon et al. [154] reported a covalent attachment of branched polyethyleneimine (PEI) to the sidewalls of SWNTs through the use of fluorinated single-wall CNTs as precursors. The structural integrity of the original purified SWNT is maintained upon covalent functionalization with PEI. Solid-state ^{13}C NMR shows the presence of carboxylate substituents due to carbamate formation as a consequence of the reversible CO_2 absorption to the primary amine substituents of the PEI. Desorption of CO_2 is accomplished by heating under argon at 75 °C, while the dependence of the quantity of CO_2 absorbed on temperature and the molecular weight of the PEI is also observed.

Besides the experimental investigation, the theoretical researches on the CO_2 capture over CNT were also reported. For example, Liu et al. [155] have shown, from molecular dynamics simulations, that the windowed CNTs are able to separate CO_2 from the CO_2/CH_4 mixture with a CO_2 permeance several orders of magnitude higher than the conventional analogs (Fig. 2.26).

The aforementioned examples open the door for the design and preparation of highly effective carbonaceous CO_2 adsorbents with controlled pore features and

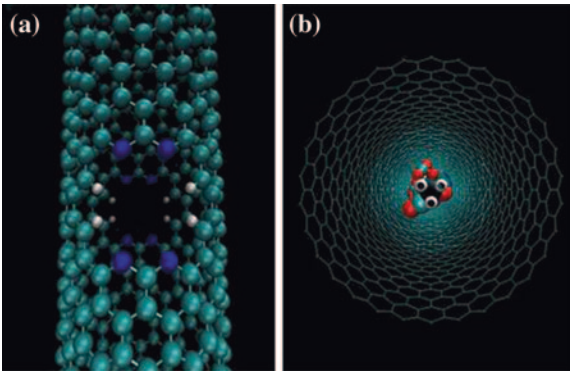

Fig. 2.26 **a** 4N4H windows or pores on the wall of the inner tube. **b** Initial setup of the simulation where CO_2/CH_4 gas mixture is inside the windowed inner tube; on the outside is a pristine tube. The following color code is adopted throughout: carbon (*cyan*), oxygen (*red*), hydrogen (*white*), and nitrogen (*blue*). Reprinted with the permission from Ref. [155]. Copyright 2012 American Chemical Society

tailored surface chemistry. These porous carbons would combine the merits of designed synthesis (controlled pore structure and task-specific surface chemistry) and intrinsic properties (excellent chemical and thermal stability, developed porosity) of carbon materials and meet the complex requirements of efficient adsorbents for CO_2 capture.

2.5.3.1 Carbon Nanofibers

Besides CNTs, another 1D carbon nanostructure is carbon nanofibers. For example, Shen et al. [156] prepared a series of hierarchical porous carbon fibers with a BET surface area of 2,231 $m^2\ g^{-1}$ and a pore volume of 1.16 $cm^3\ g^{-1}$. In this synthesis method, the polyacrylonitrile (PAN) nanofibers (prepared by dry–wet spinning) were selected as precursors, and pre-oxidation and chemical activation were involved to get the developed porosities. This type of material contained a large amount of nitrogen-containing groups (N content > 8.1 wt%) and consequently basic sites, resulting in a faster adsorption rate and a higher adsorption capacity for CO_2 than the commercial zeolite 13X that is conventionally used to capture CO_2, in the presence of H_2O (Fig. 2.27).

2.5.3.2 Carbon Nanoribbons and Nanoscrolls

Asai et al. [157] reported a new CO_2 sorption behavior over graphitic nanoribbons, which was distinctly different from the behavior of nanoporous carbon and carbon blacks. They found a remarkable irreversibility in adsorption of CO_2 and H_2O on such kind of graphitic nanoribbons at ambient temperature (Fig. 2.28).

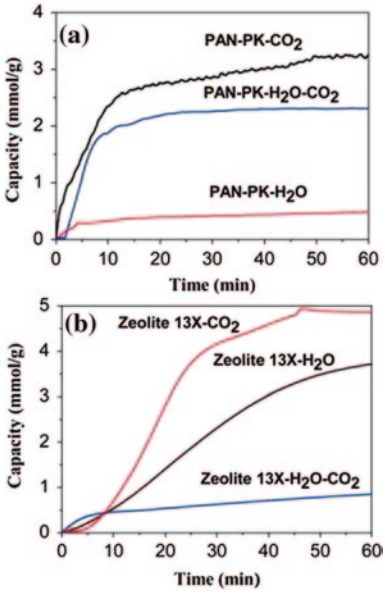

Fig. 2.27 Effect of H_2O on the adsorption of CO_2 by PAN-PK (**a**) and zeolite 13X (**b**) at 25 °C. Reproduced from Ref. [156] by permission of The Royal Society of Chemistry

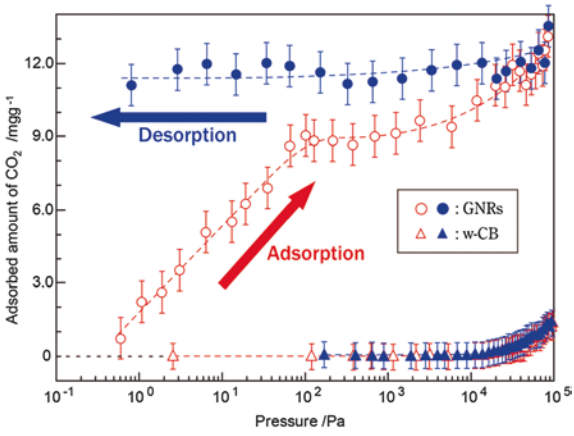

Fig. 2.28 Adsorption isotherms of CO_2 on GNRs and well-crystalline CBs at 303 K. Reprinted with the permission from Ref. [157]. Copyright 2011 American Chemical Society

The irreversible adsorptions of both CO_2 and H_2O are due to the large number of sp^3-hybridized carbon atoms located at the edges. The authors believe that the observed irreversible adsorption capacity of the edge surfaces of graphitic nanoribbons for CO_2 and H_2O indicates a high potential in the fabrication of novel types of catalysts and highly selective gas sensors.

Through molecular dynamics simulations, Mantzalis and Asproulis [158] investigated the layering behavior of carbon dioxide transported through carbon nanoscrolls. The layering arrangements were investigated for carbon nanoscrolls with interlayer distances spanning from 4.2 to 8.3 Å at temperature of 300 K and pressures ranging from 5 to 20 bars. It was shown that the number of layers, their

relative strength, and the starting point of bifurcation phenomena vary as a function of the nanoscrolls' interlayer distance, scroll's core radius, CO_2 density, and gas structure interactions. It is also shown that the number of carbon dioxide molecules adsorbed per scroll's carbon particles is a function of the scroll's surface-to-volume ratio and is maximized under certain structural configurations.

2.6 Critical Material Aspects of Porous Carbon Design on CO_2 Capture

2.6.1 Micropore Size and Volume Influences

It is highly necessary to discuss the key parameters of materials for CO_2 capture. To do this, the first thing is the selection of model carbon. Carbide-derived carbon (CDC) is such kind of carbon, which can be fabricated through hydrothermal decomposition of carbide precursors on various substrates and then selectively etching metals from metal carbides using chlorine at elevated temperature. The most attractive aspects of these materials lie in their precisely controlled micropore size (with a sub-angstrom accuracy) and tunable specific surface area (up to 3,200 $m^2\ g^{-1}$) [159–161]. This characteristics allow them to serve as carbon models for fundamental investigating the influences of micropore sizes on CO_2 adsorption. In researching hydrogen and methane adsorption over CDC, it has been shown that the sorption capability does not necessarily scale with the surface area or the pore size, but it depends on the volume of pores smaller than 1 nm. Similarly, Presser et al. [161] systematically investigate CO_2 adsorption at atmospheric and subatmospheric pressures at near-ambient temperature (0 °C) on the basis of a series of CDC with well-controlled PSD and surface areas (Table 2.3) synthesized from TiC powders.

They found that the average pore size and the total pore volume are not adequate measures to predict the CO_2 uptake of microporous carbon sorbents, the pore volume of micropores strongly governs the amount of adsorbed CO_2 [161]. Neither high surface area CDC after chemical activation (surface area 3,101 $m^2\ g^{-1}$) nor high pore volume nano-TiC-CDC (V_{total} 1.61 $cm^3\ g^{-1}$) correspond with the highest CO_2 adsorption capacity. At ambient pressure, the CO_2 uptake closely follows a linear correlation with the volume of pores smaller or equal to a diameter of 1.5 nm. Pores smaller than 0.5 nm contribute to the amount of adsorbed CO_2, but the best correlation is found for pore volume smaller than 0.8 nm (Fig. 2.29). The correlation between the amount of adsorbed CO_2 at low partial pressures and volume of smaller pores is the basis for the well-known application of CO_2 sorption as a method to calculate the pore characteristics of microporous materials. Subatmospheric pressures are of particular interest for industrial applications, where partial pressure of CO_2 is below 1 bar, and here, the best prediction of the CO_2 uptake capacity at 0.1 bar would be based on the volume of pores smaller or equal to a diameter of 0.5 nm (Fig. 2.29). This correlation can be used to design better CO_2 sorbents and CCS devices.

Table 2.3 Pore characteristics and CO_2 uptake at 0.1 and 1.0 bar for nano-TiC-CDC, micro-TiC-CDC and activated micro-TiC-CDC

Sample	Chlorination temperature (°C)	Annealing atmosphere temperature (°C)	Mean pore* size (nm)	DFT SSA* (m^2/g)	BET SSA* (m^2/g)	Total pore volume* (cm^3/g)	CO_2 uptake @0.1 bar** (mol/kg)	CO_2 uptake @1 bar** (mol/kg)
Nano-Tic-CDC	200	H_2@200	0.56	336	324	0.26	0.86	2.15
	200	H_2@600	0.58	444	434	0.36	1.10	2.74
	400	H_2@400	0.62	780	740	0.54	1.13	3.26
	400	H_2@600	0.69	1,038	1,002	0.73	0.90	3.47
	600	H_2@600	0.85	843	952	0.81	0.54	2.54
	800	H_2@600	0.86	1,624	1,855	1.22	0.75	4.23
	1,000	H_2@600	0.96	1,674	1,920	1.61	0.62	3.70
	1,200	H_2@600	1.15	563	619	0.88	0.10	1.40
Micro-Tic	200	H_2@200	0.52	582	497	0.23	0.89	2.82
	400	H_2@600	0.53	968	910	0.30	1.15	3.90
	600	H_2@600	0.60	1,294	1,383	0.56	1.62	6.23
	700	H_2@600	0.66	2,015	1,832	0.84	1.51	7.09
	800	H_2@600	0.80	1,687	1,772	0.72	1.56	6.79
	1,000	H_2@600	0.78	1,662	1,669	0.75	1.18	5.45
	1,200	H_2@600	0.94	1,319	1,540	0.86	0.68	3.34
Activated micro-TIC-CDC	600	vacuum@1,500	0.85	1,589	1,776	0.87	1.06	4.77
	800	NH_3@600	0.76	1,840	2,094	0.78	1.15	5.33
	400	KOH@600	0.72	2,628	2,911	0.92	1.06	5.91
	500	KOH@600	0.96	2,778	3,101	0.97	1.18	6.31
	800	KOH@600	0.79	2,300	2,565	1.05	1.31	6.92
	600	CO_2@875	0.69	2,037	1,810	0.70	1.54	6.79
	600	CO_2@925	0.82	2,167	2,468	0.99	1.19	5.97
	600	CO_2@950	0.83	2,142	2,489	1.00	1.03	5.42
	600	CO_2@960	0.83	2,045	2,229	0.88	1.27	6.18

*Data derived from N_2 sorption

**Data derived from CO_2 sorption

Reproduced from Ref. [161] by permission of The Royal Society of Chemistry

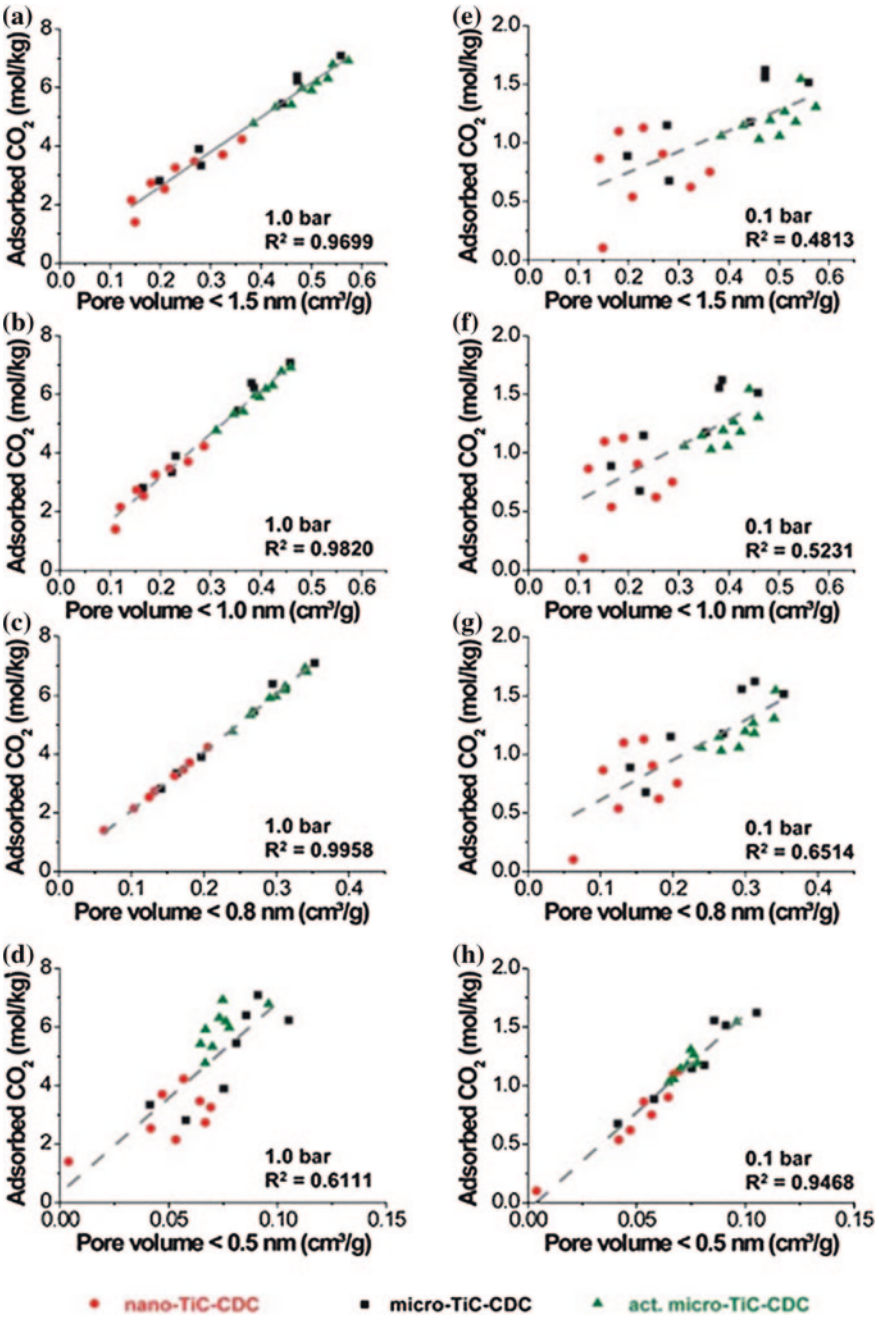

Fig. 2.29 CO_2 uptake at 0 and 1.0 bar (**a**–**d**) and 0.1 bar (**e**–**h**) for the volume of pores smaller 1.5 nm (**a**, **e**), 1.0 nm (**b**, **f**), 0.8 nm (**c**, **g**), and 0.5 nm (**d**, **h**). Reproduced from Ref. [161] by permission of The Royal Society of Chemistry

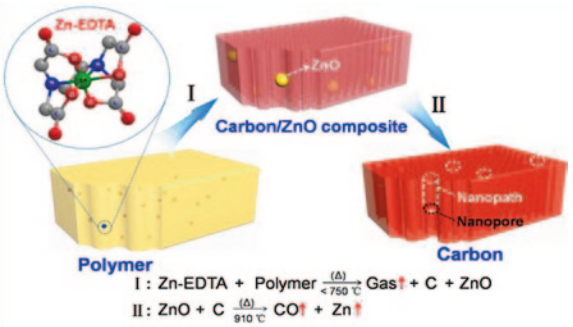

Fig. 2.30 Synthesis principle of microporous carbon using zinc species as dynamic molecular porogens for the creation of abundant microporosity. Reproduced from Ref. [162] by permission of John Wiley & Sons Ltd

The important role of micropores on CO_2 capture has been widely accepted. Therefore, besides the above-mentioned ways, i.e., hard template methods (e.g., zeolites as templates), CDC pathways, and so on, new strategies to fabricate such pore systems are highly expected. For instance, Qian et al. [162] report a novel synthesis approach for the fabrication of microporous carbon materials (HCMs) by using discrete chelating zinc species as dynamic molecular porogens to create extra micropores that enhance their CO_2 adsorption capacity and selectivity. During carbonization process, the evaporation of the in situ formed Zn species would create additional nanopaths that contribute to the additional micropore volume for CO_2 adsorption (Fig. 2.30).

The resulted HCMs show increased amount of micropores with sizes in the range of 0.7–1.0 nm, and a high CO_2 adsorption capacity of 5.4 mmol g^{-1} (23.8 wt%) at 273 K and 3.8 mmol g^{-1} (16.7 wt%) at 298 K and 1 atm, which are superior to most carbon-based adsorbents with N-doping or high specific surface area. As shown in Fig. 2.31, the dynamic gas separation measurement, using 16 % (v/v) CO_2 in N_2 as feedstock, demonstrates that CO_2 can be effectively separated from N_2 under ambient conditions and shows a high separation factor ($S_{CO2/N2} = 110$) for CO_2 over N_2, reflecting a strongly competitive CO_2 adsorption capacity. When the feedstock contains water vapor, the dynamic capacity of CO_2 is almost identical as that measured under dried conditions, indicating the carbon material has an excellent tolerance to humidity. An easy CO_2 release can be realized by purging an argon flow through the fixed-bed adsorber at 298 K, indicating the good regeneration ability.

2.6.2 Heteroatoms Doping Influences

Besides micropores, the heteroatom doping is another possible factor that may influence the CO_2 adsorption behavior. Among them, the influence of N-doping is reported most frequently. A wide range of N-doped carbons with diverse morphologies have been developed and tested for CO_2 capture. The N-doping ways can be broadly classified into three categories: (1) using nitrogen-containing precursors and pyrolysis; (2) high-temperature reaction and transformation based on pre-made carbons, i.e., NH_3 activation; (3) direct loading of liquid amines into the pores of pre-made carbons. For the first two approaches, the introduction of nitrogen-containing

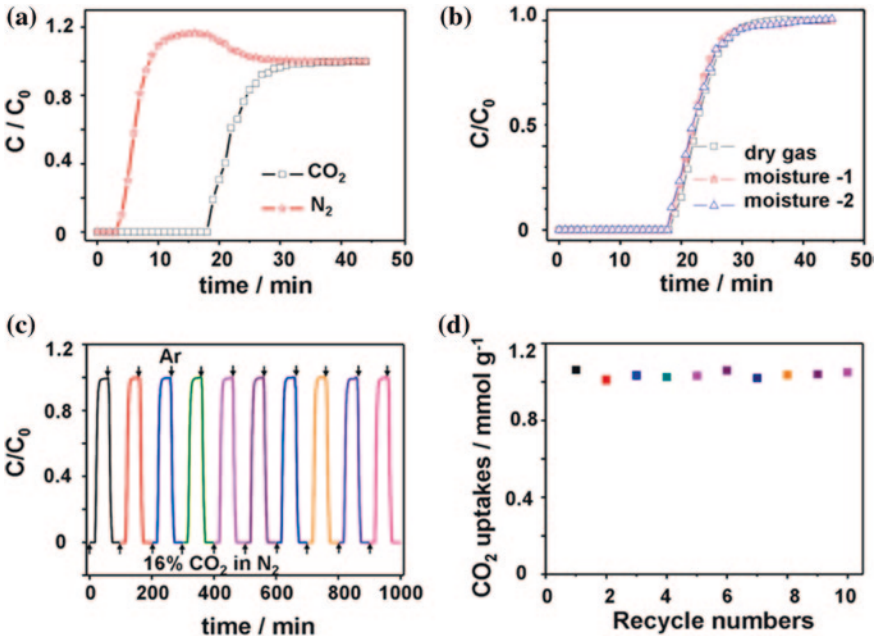

Fig. 2.31 **a** Breakthrough curve of HCM-ZC-1 using a stream of 16 % (v/v) CO_2 in N_2 at 25 °C; **b** breakthrough curve of CO_2 under a moisture condition; **c** recycle runs of CO_2 adsorption–desorption on HCM-ZC-1 at 25 °C, using a stream of 16 % (v/v) CO_2 in N_2, followed by a regeneration under argon flow; **d** CO_2 uptake of each adsorption run. Reproduced from Ref [162] by permission of John Wiley & Sons Ltd

functional groups has little effect on pore structures, and these functional groups are highly dispersed either in the surface or in the carbon matrix. For the third way, a high concentration of functional groups can be obtained; however, a large part of pores will be blocked by filling of liquid amines. As regards to the role of heteroatom-involving sites, particularly N-containing groups in CO_2 capture, it still remains controversial. At present, there are three viewpoints regarding this issue: acid–base interactions, hydrogen-bonding interaction, and electrostatic interactions. The role of heteroatoms is discussed along with the review of each type of porous carbons.

2.6.2.1 Using Nitrogen-Containing Precursors

The rationally selected polymeric carbon precursors mainly involve *p*-diaminobenzene [163], polyacrylonitrile [164], melamine [165], and so on. Zhao et al. [163, 166] have prepared a series of nitrogen-doped carbon materials with a very high nitrogen doping concentration (ca. 13 wt%) and rich micropores (<1 nm), which lend them the highly desired characteristics for selective CO_2 capture. For example, they reported a nitrogen-doped mesoporous carbon materials (Fig. 2.32) that can be nanocasted from tri-continuous mesoporous silica (IBN-9) by using a mixed

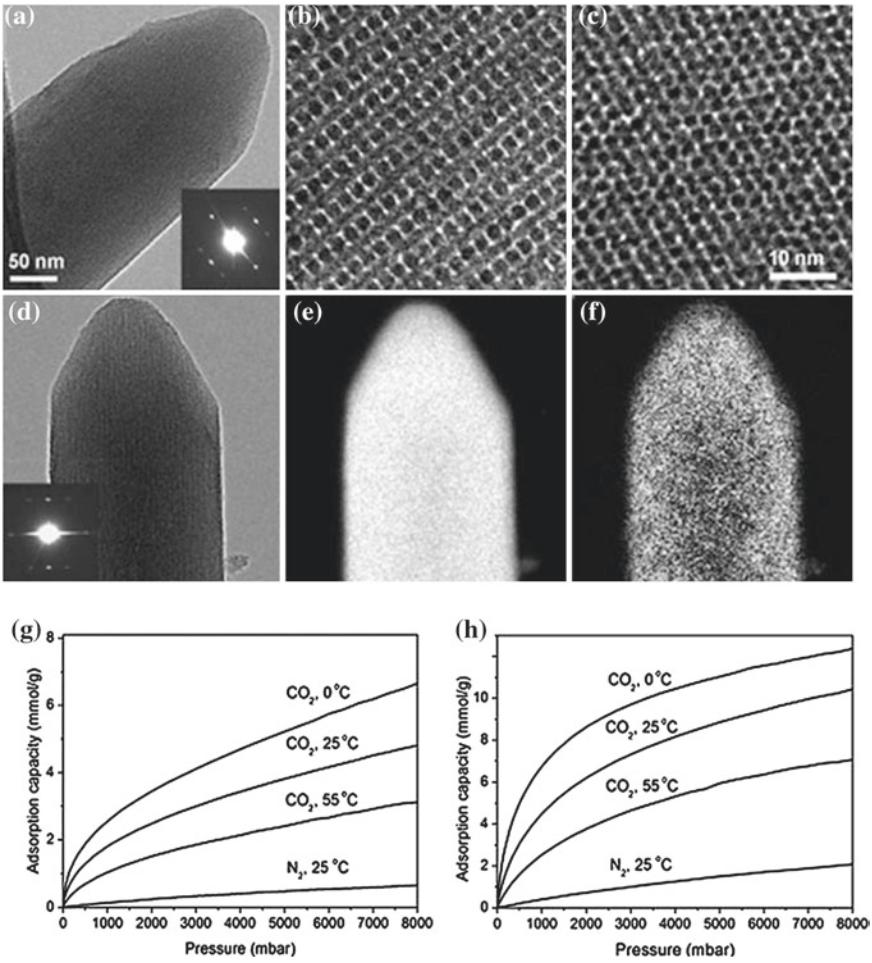

Fig. 2.32 **a**, **d** TEM images and SAED patterns (*insets*) of IBN9-NC (**a**) and IBN9-NC1 (**d**) taken along the [100] direction. **b**, **c** High-resolution TEM images of IBN9-NC taken along the [100] (**b**) and [110] (**c**) directions. **e**, **f** Energy-filtered TEM images of the particle in (**d**), showing carbon mapping (**e**) and nitrogen mapping (**f**). Images **d**–**f** have the same magnification as image (**a**); image (**b**) has the same magnification as image (**c**). CO_2 adsorption isotherms at 0, 25, and 55 °C and N_2 adsorption isotherm at 25 °C of IBN9-NC1 (**g**) and IBN-9-NC1-A (**h**). Reproduced from Ref. [163] by permission of The Royal Society of Chemistry

carbon precursor comprised of nitrogen-containing p-diaminobenzene and nitrogen-free furfural alcohol. After a chemical activation process, a high content of nitrogen and a large proportion of micropores in one material were integrated. The optimized material exhibited excellent adsorption properties in terms of both CO_2 uptake and CO_2/N_2 selectivity (Fig. 2.32). Particularly, its CO_2 adsorption uptake in the typical condition of flue gas (e.g., CO_2 partial pressure of 0.2 bar, 25 °C) is as high as 1.75 mmol g^{-1}, which is far superior to most reported carbon materials. These new

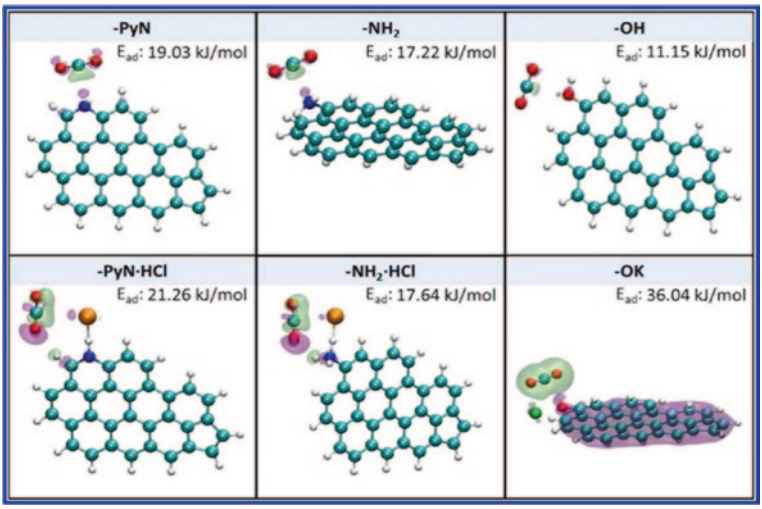

Fig. 2.33 Optimized configurations of CO_2 adsorption on carbon clusters with different polar groups (*cyan* C; *white* H; *blue* N; *red* O; *light green* K) and the corresponding contour plots of the differential charge density. The contour value is ±0.001. The *purple* and *lime* regions represent the charge accumulation and charge depletion regions, respectively. Reprinted with the permission from Ref. [166]. Copyright 2012 American Chemical Society

materials showed high CO_2 adsorption heats (ca. 40 kJ mol^{-1} at initial adsorption stages), suggesting an enhanced physical adsorption effect by nitrogen doping [163].

Later, they designed and prepared a series of porous carbons, including microporous carbon, mesoporous carbon, which are used for selective CO_2 capture. The authors found that the combination of a high N-doping concentration (>10 wt%) and extra-framework cations endowed N-doped microporous carbons with exceptional CO_2 adsorption capabilities, especially at low pressures (CO_2 uptake of 1.62 mmol g^{-1} at 25 °C and 0.1 bar) [166]. Single component adsorption isotherms indicated that its CO_2/N_2 selectivity was 48, which also significantly surpasses the selectivity of conventional carbon materials. Furthermore, the dynamical breakthrough experiments using CO_2/N_2 (10:90 v/v) mixtures reveal that the CO_2/N_2 selectivity was as high as 44, comparable to that predicted from equilibrium adsorption data. More interestingly, they conducted theoretical calculations that correlate the polarizing capabilities of various functional groups (K^+, Cl^- ions as well as N-containing sites, see Fig. 2.33) with their enhancement effects on CO_2 adsorption and demonstrated that such effects are essentially based on electrostatic interactions. This represents a new perspective to explain the positive role of heteroatoms in contribution to a high CO_2 uptake.

Kowalewski et al. [167] reported another type of nitrogen-enriched porous carbon nanostructure as CO_2 capture materials, which has been prepared via the carbonization of polyacrylonitrile containing block copolymer. The typical sample exhibited good selectivity for CO_2 manifested by sevenfold to tenfold larger amount of adsorbed CO_2 over N_2 (Fig. 2.34). The analysis of isosteric heats of CO_2 adsorption

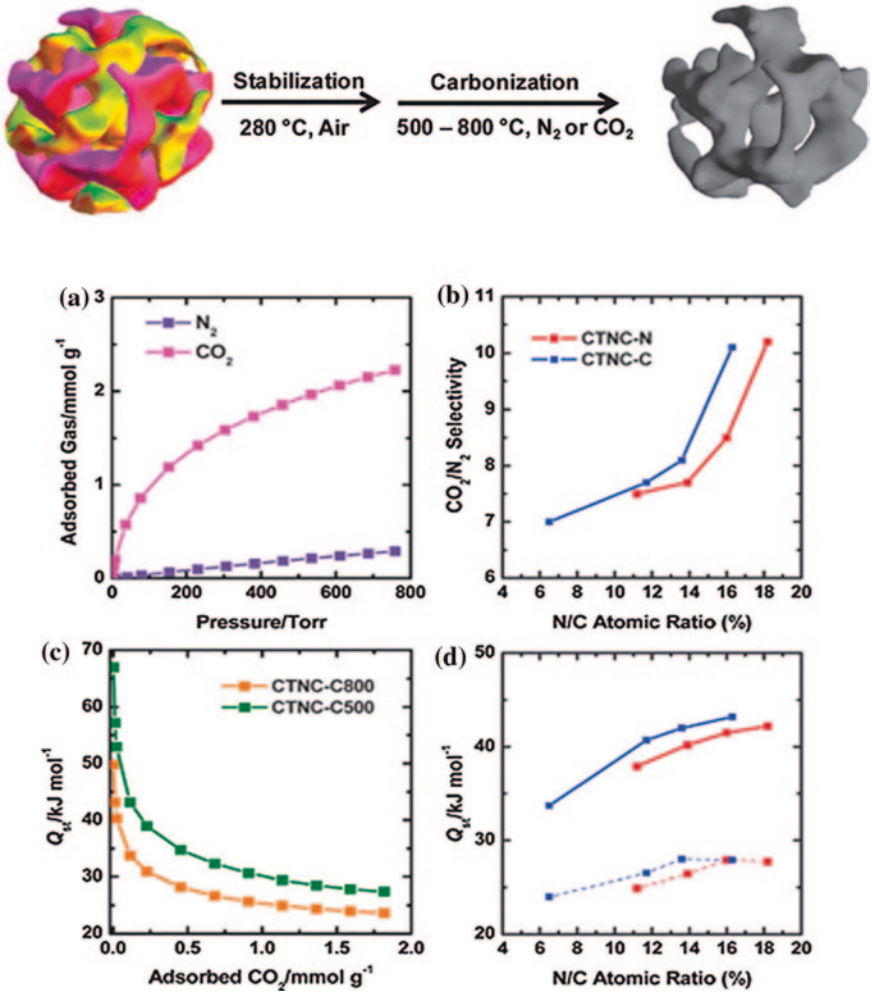

Fig. 2.34 *Up* Synthetic route for CTNC. *Bottom* **a** Comparison of 25 °C adsorption isotherms of CO_2 and N_2 for CTNC-N700; **b** correlation between CO_2/N_2 selectivity and N/C atomic ratio; **c** isosteric heats of CO_2 adsorption (Q_{st}) by CTNC-C500 and CTNC-C800; **d** correlation between Q_{st} and N/C atomic ratio at different CO_2 coverages (*red* CTNC-N; *blue* CTNC-C; *solid line* 0.1 mmol g^{-1} of CO_2 adsorbed; *dash line* 1.8 mmol g^{-1} of CO_2 adsorbed). Reproduced from Ref. [167] by permission of The Royal Society of Chemistry

also leads to similar conclusions about the role of surface nitrogens. The characteristic initial sharp decrease to the plateau observed in these curves is likely indicative of initial adsorption driven by more active nitrogen surface sites. As shown in Fig. 2.34, for any given nitrogen content, N-doped sample exhibited higher selectivity and Q_{st} than non-N-doped counterpart. By this in-depth analysis, they believe that the adsorption capacity can be increased by enlarging the surface area under CO_2 treatment at lower temperatures (<700 °C); while CO_2 treatment at a higher temperature

(800 °C) produced even more significant increase in surface area and CO_2 capacity but reduced selectivity, due to the loss of nitrogen.

Recently, Nandi and coworkers have fabricated a series of highly porous N-doped porous carbon monoliths as CO_2 capture materials. This series of N-doped carbons were obtained from the mesoporous PAN monolith via thermal treatment in two steps (Fig. 2.35) [164]. The monoliths were pre-treated in air at 503 K for activation, which led to cyclization inside the polymer framework, generating a ladder polymer. Then, the ladder polymer gradually underwent aromatization, generating an aromatic ladder. In the next heating step, the aromatized polymer was converted to its carbon with a lamellar phase by carbonization in Ar or an Ar-CO_2 mixture. CO_2 adsorption isotherms (Fig. 2.35) show reversible adsorption characteristics indicating weak interaction of CO_2 molecules with the pore walls. More impressively, these carbon monoliths show unprecedentedly high CO_2 uptake of 5.14 mmol g^{-1} at ambient pressure and temperature and 11.51 mmol g^{-1} at ambient pressure and 0 °C. As shown in Fig. 2.35, the typical sample shows high initial Q_{st} values of up to 65.2 kJ mol^{-1}. High initial isosteric heats of adsorption (Q_{st}) values indicate strong adsorbent–adsorbate interaction between the N-containing carbon framework and CO_2 molecules.

2.6.2.2 High-Temperature Reaction and Transformation

Treating as-made porous carbons with gaseous ammonia under a high temperature (e.g., 900 °C) is another popular way for preparation of N-doped carbon. In principle, the reaction with ammonia is expected to take place at carboxylic acid sites formed by the oxidation of side groups and the ring system. At a high temperature, ammonia decomposes with the formation of radicals, such as NH_2, NH, and H [168, 169]. These radicals may react with the carbon surface to form functional groups, such as –NH_2, –CN, pyridinic, pyrrolic, and quaternary nitrogen.

Many researchers believe that the introduction of nitrogen will increase basicity of carbons and thus will facilitate the removal of trace amounts of acidic gases including CO_2. For example, Przepiórski et al. [170] found that high-temperature ammonia treatment of activated carbon clearly enhance the CO_2 adsorption. In their work, the ammonia treatment was performed for 2 h at elevated temperatures ranging from 200 to 1,000 °C. The CO_2 capture tests confirm that the adsorption of CO_2 was enhanced by ammonia treatment. The enhancement was attributed to the presence of C–N and C=N groups. And further, the largest CO_2 uptake was found to be at 400 °C of the ammonia treatment temperature. From their opinion, the higher temperature treatment may cause the close of micropores or changes in the size of pores.

Pevida et al. [171] demonstrated that ammonia treatment at temperatures higher than 600 °C incorporated nitrogen mainly into aromatic rings, while at lower temperatures nitrogen was introduced into more labile functionalities, such as amide-like functionalities. The CO_2 capture capacities at 25 °C of the treated carbons increased with respect to the parent carbons. In particular, after ammonia modification at 800 °C, the CO_2 capture capacities of wood-derived carbons rose from 7.0 to 8.4 wt%. It is worth pointing out that it is the specific nitrogen functionalities rather

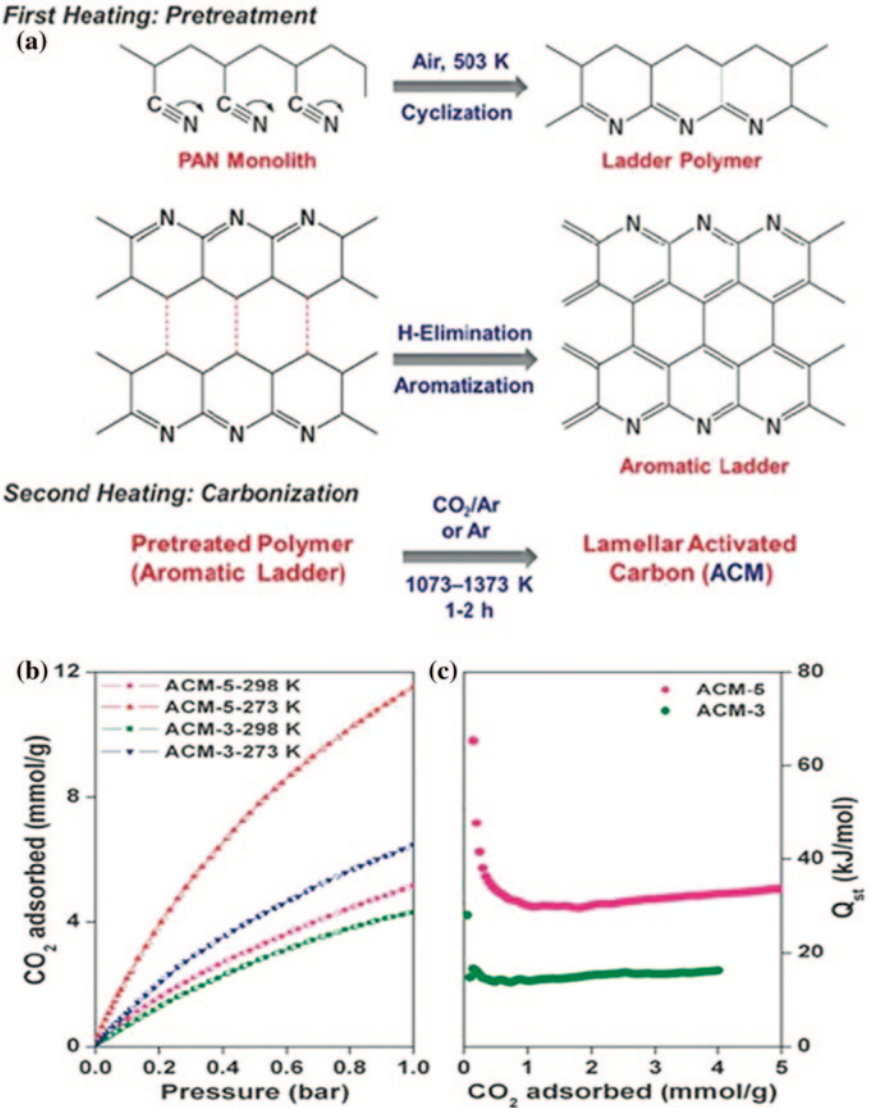

Fig. 2.35 **a** Carbonization of PAN monolith. **b** CO_2 sorption up to 1 bar, at 273 K and 298 K: adsorption (*filled symbols*) and desorption (*empty symbols*). **c** Isosteric heat of CO_2 adsorption (Q_{st}) as a function of CO_2 adsorbed. Reproduced from Ref. [164] by permission of The Royal Society of Chemistry

than the total nitrogen content that are responsible for increasing the CO_2-adsorbent affinity. The same group also investigated the ammonia treatment of pristine carbons in the presence of air (ammoxidation) [172]. They found that, during ammoxidation (amination in the presence of air), the formation of nitriles and amide-like functionalities were favoured and a great amount of nitrogen was incorporated onto the carbon surface. Further, nitrogen uptake by ammoxidation at 300 °C was found to be

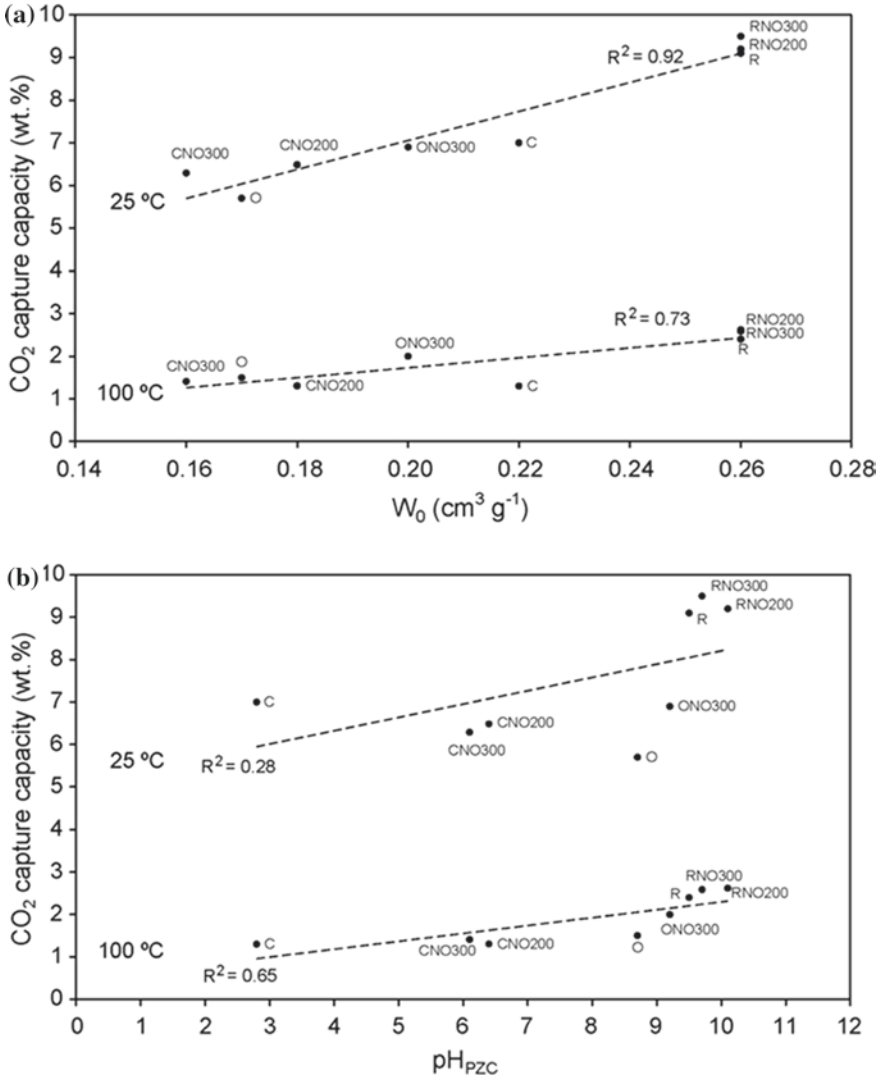

Fig. 2.36 Relationship between the CO_2 capture capacity and: **a** the narrow micropore volume, W_0, and **b** the point of zero charge, pH_{PZC}. Reprinted from Ref. [172]. Copyright 2010, with permission from Elsevier

proportional to the oxygen content of the starting carbon. Ammonia seems to react preferentially with the CO_2-evolving groups of the starting carbon, such as carboxyls, while the remaining oxygen mainly forms part of CO-evolving groups, such as amides or lactams. CO_2 capture result shows that CO_2 capture capacity is related to the narrow micropore volume of the samples, and this relationship is approximately linear at room temperature (Fig. 2.36). However, above room temperature, the trend deviates from linearity due to the possible influence of surface basicity.

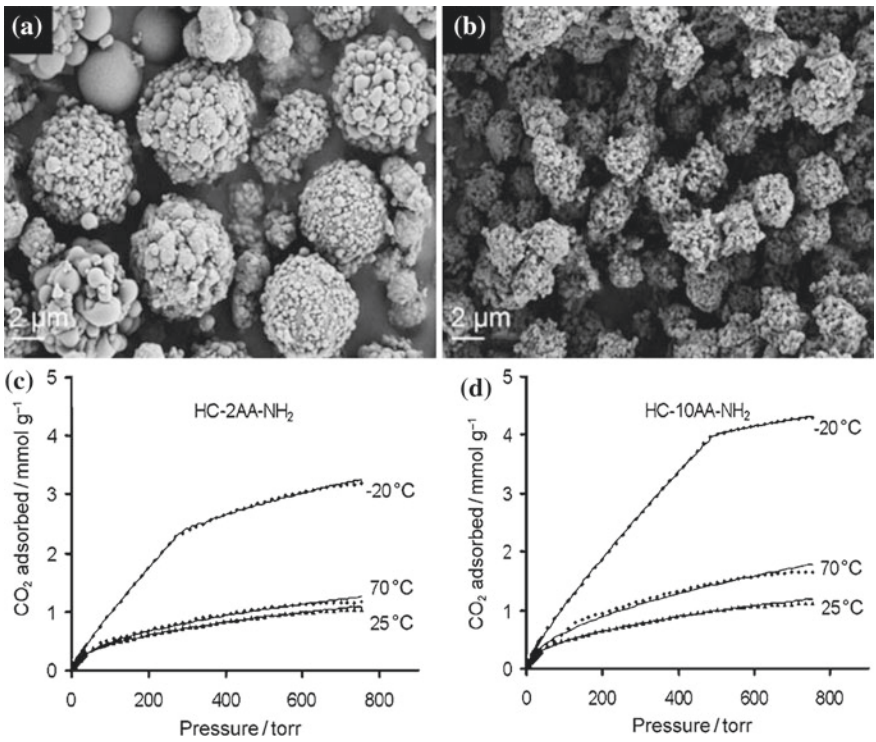

Fig. 2.37 SEM images of amine-rich carbonaceous materials: **a** HC-2AA-NH_2, and **b** HC-10AA-NH_2. The numbers 2 and 10 refer to the amounts of acrylic acid (AA) relative to the total amount of glucose (in wt%). Temperature- and pressure-dependent CO_2 uptake of **c** HC-2AA-NH_2 and **d** HC-10AA-NH_2. The *lines* are numerical estimates using Freundlich models (one- or two-site). 1 torr = 1.333×10^2 Pa. Reproduced from Ref. [175] by permission of John Wiley & Sons Ltd

2.6.2.3 Impregnation with Liquid Amines

Inspired with silica-based hybrid sorbents (molecular basket) with grafted or impregnated amine groups on porous silica substrates [173, 174], Zhao et al. reported an aminated adsorbents generated from sustainable biomass (glucose) [175]. Two steps are involved in this synthesis: (1) HTC of glucose; (2) transformation into porous carbon–amine composite by a post-synthetic modification with a branched tetramine. The authors first prepared the substrate carbons with novel raspberry morphology, which may be beneficial for the loading of liquid amines. Interestingly, the raspberry morphology is maintained after modification of the carbons with grafted polyamines, as illustrated in the SEM images in Fig. 2.37.

CO_2 capture results show a very high CO_2 uptake (up to 4.3 mmol g^{-1}) at −20 °C (Fig. 2.37). More importantly, this type of composites delivered a very high CO_2 selectivity at low (–20 °C, CO_2/N_2 of 65–85) and high (70 °C, CO_2/N_2 of 90–110) temperatures. These high capacities and selectivities are consistent

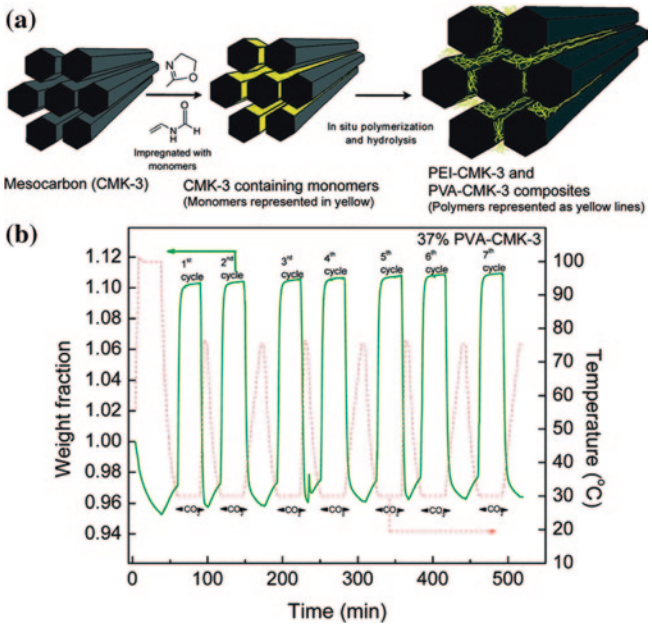

Fig. 2.38 **a** Synthesis processes to produce mesoporous polymer–carbon composites PEI-CMK-3 and PVA-CMK-3. **b** Sorption cycles of CO_2 studied by TGA at 30 °C on the 37 % PVA-CMK-3 sorbent. Reprinted with the permission from Ref. [176]. Copyright 2011 American Chemical Society

with the high amine loadings. The high capacity is remarkable given that the prepared absorbents have only a moderately large specific surface area. Clearly, some of the CO_2 absorbs within the amine-rich, liquid-grafted surface layer. Thus, a more ideal CO_2 capture material can be imagined with a high active amine content combined with a more optimized channel.

It should be noted that the introduction of liquid amines through impregnation might result in some other negative effects, such as blockage of pores, the unstable basic sites on the surface in long time cycling. To address this issue, Tour's group developed a route to synthesize polymer–mesocarbon composites that would lead to higher degrees of CO_2 adsorption by the in situ polymerization of amine species to produce polyethylenimine (PEI) and polyvinylamine (PVA) inside the mesocarbon CMK-3 (Fig. 2.38) [176]. This structured composites exhibit high stability due to the formation of interpenetrating composite frameworks between the entrapped polymers and mesocarbon CMK-3. CO_2 uptake measurements showed that the 39 % PEI-CMK-3 composite had ca. 12 wt% CO_2 uptake capacity and the 37 % PVA-CMK-3 composite had ca. 13 wt% CO_2 uptake capacity at 30 °C and 1 atm. More importantly, the composite can easily be regenerated at 75 °C and cycles stably (even up to 500 min, see Fig. 2.38).

Besides the most commonly investigated N-containing functional groups, the oxygen-containing or sulfur-containing functional groups were also investigated

to enhance CO_2 adsorption in microporous carbon materials, particularly in the absence of water vapor, and the hydrated graphite was found to hinder CO_2 adsorption [177]. Liu and Wilcox [178] theoretically analyzed the role of oxygen-containing groups in CO_2 capture based on an assumption, in which complex pore structures for natural organic materials (e.g., coal and gas shale) and carbon-based porous materials are modeled as a collection of independent, non-interconnected, functionalized graphitic slit pores with surface heterogeneities. Electronic structure calculations coupled with van der Waals-inclusive corrections have been performed to investigate the electronic properties of functionalized graphitic surfaces. With Bader charge analysis, electronic structure calculations can provide the initial framework comprising both the geometry and corresponding charge information required to carry out statistical modeling. Grand canonical Monte Carlo simulations were carried out to determine the adsorption isotherms for a given adsorbent–adsorbate interaction at temperature/pressure conditions relevant to carbon capture applications to focus on the effect of the surface functionalities.

With the above-mentioned simulation techniques, the authors summarized the results in Fig. 2.39. The main points include: (1) the CO_2 molecules are more organized and aligned when they are adsorbed in the functionalized slit pores, and thus, the adsorption capacity is enhanced by the higher efficient side-by-side packing; (2) in the ultramicropores (less than 7 Å), due to the overlapping potentials from the strong pore wall−wall interactions and the strong CO_2−wall interaction, the condensed adsorbed-CO_2 density is even higher than that of the larger pores.

In general, as the pore width decreases, the surface functionalities dictate the adsorption, and thus, the surface functionalities play a more important role in increasing the CO_2 adsorption capacity. The surface heterogeneity changes the adsorbates' accumulation configuration by changing the geometry of the pore surface and the charge distribution of the surface, which is consistent with the Bader charge results of DFT study. Also, other molecular-level simulations of CO_2 adsorption behavior in micropores of porous carbons show that heteroatom doping greatly enhances CO_2 uptake and selectivity at low coverage [179]; while the CO_2 capture performance of porous carbons at high pressure is largely dependent on their structure parameters.

2.7 Summary and Outlook

In summary, porous carbon-based materials for CO_2 capture have experienced rapid development in the last several decades and will continue to blossom. The requirements of CO_2 captures vary a lot depending on different processes, namely post-combustion (low pressure, predominantly CO_2/N_2 separation), pre-combustion (high pressure, predominantly CO_2/H_2 separation) capture and natural gas sweetening (predominantly CO_2/CH_4 separation). Thus, various kinds of new carbon materials with defined textural properties as well as tailored surface chemistry have been synthesized for a specific CO_2 capture process. Another advantage lies

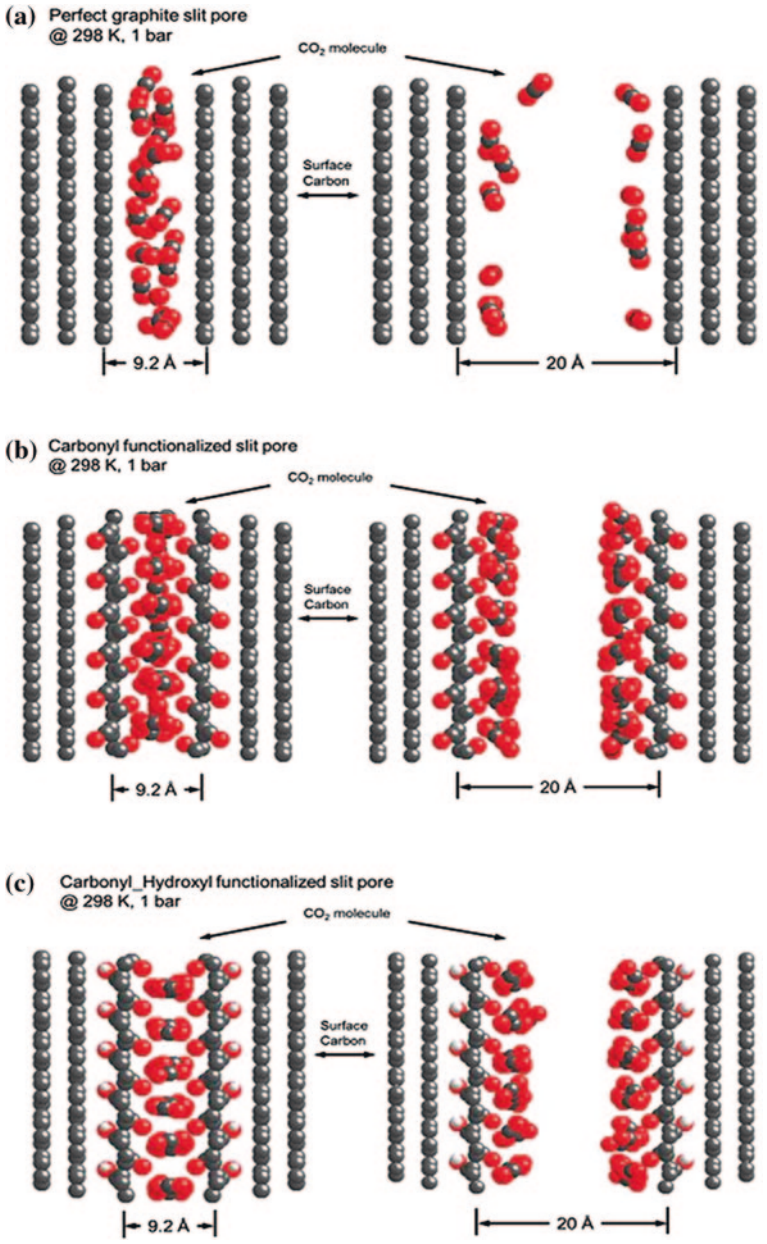

Fig. 2.39 Comparisons of CO_2 adsorbed in functionalized micropores with that in the perfect graphite slit pore: *left* side views of adsorbed CO_2 in various functionalized graphite slit pores with pore width of 9.2 Å; *right* side views of adsorbed CO_2 in various functionalized graphite slit pores with pore width of 20 Å. Reprinted with the permission from Ref. [178]. Copyright 2012 American Chemical Society

in the relatively hydrophobic properties, which ensure a high capacity even under hydrated condition. Although much progress has been made, many challenges still exist from both scientific and technological points of view.

Firstly, there are completely irregular features over nanometer length scale. Researchers should pay more attention to the in-depth understanding of the physics and chemistry of carbon, which is highly important for the design and synthesis of tailored porous carbons as next-generation CO_2 capture materials and model carbons for fundamental investigations. For example, the important scientific issues may include the contribution of pores in different length scale (micro-, meso-, and macropores) to CO_2 capture capability, the CO_2 molecules transport behavior in pore systems, and so on. These depend on the development of advanced characterization methods, which can support, guide and provide further refinement to the most promising structures. For instance, the solid-state NMR techniques can provide reliable information regarding CO_2 diffusion at molecular scale. From this measurement, researchers can correlate microscopic absorbate dynamics with the structural information on the basis of one kind of carbon model after CO_2 loading. By comparing the behaviors of the microscopic mobility and the macroscopic diffusion, one can get an insight into the mechanism of selective transport through these materials.

Secondly, the mechanism as well as the contribution of surface heterogeneity (e.g., N-, S-doped sites) for CO_2 binding is controversial. Up to now, the reported carbonaceous CO_2 capture materials show great complexity in pore structures and, in particular, in composition and surface chemistry (functional groups binding and dispersion in accessible surface). Thus, this condition put a big obstacle to achieve a reliable understanding of the specific contribution of each parameter. Therefore, along with developed characterizations, computational predication based on an ideal structure may be also needed.

Thirdly, the evaluation for CO_2 capture should be conducted under a simulated or even an actual flue gas condition, rather than the most often used equilibrium CO_2 sorption for the current studies. In our opinion, the international facilities in this field should create the benchmarking materials and further the prototypical materials column, which can be used for the evaluation of the CO_2 capture performance of newly emerging capture materials on the same standards. Beyond these considerations, the engineering economics of the new materials must be evaluated upon the scale-up of the materials for industrial applications, and economic models must be established to cover lifecycle CO_2 separation, capture, and sequestration costs for various technologies.

Acknowledgments This work was financially supported by the National Natural Science Foundation of China (No. 21225312) and the National Basic Research Program of China (No. 2013CB934104).

References

1. Rodríguez-Reinoso F (1998) The role of carbon materials in heterogeneous catalysis. Carbon 36:159–175
2. Kyotani T (2006) Synthesis of various types of nano carbons using the template technique. Bull Chem Soc Jpn 79:1322–1337
3. Himeno S, Komatsu T, Fujita S (2005) High-pressure adsorption equilibria of methane and carbon dioxide on several activated carbons. J Chem Eng Data 50:369–376
4. Olivares-Marín M, Maroto-Valer M (2012) Development of adsorbents for CO_2 capture from waste materials: a review. Greenhouse Gas Sci Technol 2:20–35
5. Wang R, Wang P, Yan X, Lang J, Peng C, Xue Q (2012) Promising porous carbon derived from celtuce leaves with outstanding supercapacitance and CO_2 capture performance. ACS Appl Mater Interfaces 4:5800–5806
6. Xing W, Liu C, Zhou Z, Zhang L, Zhou J, Zhuo S, Yan Z, Gao H, Wang G, Qiao SZ (2012) Superior CO_2 uptake of N-doped activated carbon through hydrogen-bonding interaction. Energy Environ Sci 5:7323–7327
7. Wang J, Heerwig A, Lohe MR, Oschatz M, Borchardt L, Kaskel S (2012) Fungi-based porous carbons for CO_2 adsorption and separation. J Mater Chem 22:13911–13913
8. Shen W, He Y, Zhang S, Li J, Fan W (2012) Yeast-based microporous carbon materials for carbon dioxide capture. ChemSusChem 5:1274–1279
9. Marco-Lozar JP, Kunowsky M, Suárez-García F, Carruthers JD, Linares-Solano A (2012) Activated carbon monoliths for gas storage at room temperature. Energy Environ Sci 5:9833–9842
10. Thote JA, Iyer KS, Chatti R, Labhsetwar NK, Biniwale RB, Rayalu SS (2010) *In situ* nitrogen enriched carbon for carbon dioxide capture. Carbon 48:396–402
11. Sevilla M, Valle-Vigón P, Fuerte AB (2011) N-doped polypyrrole-based porous carbons for CO_2 capture. Adv Funct Mater 21:2781–2787
12. White RJ, Budarin V, Luque R, Clark JH, Macquarrie DJ (2009) Tuneable porous carbonaceous materials from renewable resources. Chem Soc Rev 38:3401–3418
13. Grzyb B, Hildenbrand C, Berthon-Fabry S, Bégin D, Job N, Rigacci A, Achard P (2010) Functionalisation and chemical characterisation of cellulose-derived carbon aerogels. Carbon 48:2297–2307
14. ElKhatat AM, Al-Muhtaseb SA (2011) Advances in tailoring resorcinol-formaldehyde organic and carbon gels. Adv Mater 23:2887–2903
15. Titirici MM, Thomas A, Antonietti M (2007) Back in the black: hydrothermal carbonization of plant material as an efficient chemical process to treat the CO_2 problem? New J Chem 31:787–789
16. Titirici MM, Antonietti M, Baccile N (2008) Hydrothermal carbon from biomass: a comparison of the local structure from poly-to monosaccharides and pentoses/hexoses. Green Chem 10:1204–1212
17. Titirici MM, White RJ, Falco C, Sevilla M (2012) Black perspectives for a green future: hydrothermal carbons for environment protection and energy storage. Energy Environ Sci 5:6796–6822
18. Sevilla M, Fuertes AB (2011) Sustainable porous carbons with a superior performance for CO_2 capture. Energy Environ Sci 4:1765–1771
19. Sevilla M, Falco C, Titirici M-M, Fuertes AB (2012) High-performance CO_2 sorbents from algae. RSC Adv 2:12792–12797
20. Gaweł B, Gaweł K, Øye G (2010) Sol–gel synthesis of non-silica monolithic materials. Materials 3:2815–2833
21. Kadib AE, Chimenton R, Sachse A, Fajula F, Galarneau A, Coq B (2009) Functionalized inorganic monolithic microreactors for high productivity in fine chemicals catalytic synthesis. Angew Chem Int Ed 48:4969–4972
22. Davis ME (2002) Ordered porous materials for emerging applications. Nature 417:813–821

23. Yuan Z-Y, Su B-L (2006) Insights into hierarchically meso–macroporous structured materials. J Mater Chem 16:663–667
24. Lu AH, Hao GP (2013) Porous materials for carbon dioxide capture. Annu Rep Sect A: Inorg Chem 109:484–503
25. Lu A-H, Schüth F (2006) Nanocasting: a versatile strategy for creating nanostructured porous materials. Adv Mater 18:1793–1805
26. Lee J, Kim J, Hyeon T (2006) Recent progress in the synthesis of porous carbon materials. Adv Mater 18:2073–2094
27. Hoheisel TN, Schrettl S, Szilluweit R, Frauenrath H (2010) Nanostructured carbonaceous materials from molecular precursors. Angew Chem Int Ed 49:6496–6515
28. Tao Y, Endo M, Kaneko K (2009) Hydrophilicity-controlled carbon aerogels with high mesoporosity. J Am Chem Soc 131:904–905
29. Silva AMT, Machado BF, Figueiredo JL, Faria JL (2009) Controlling the surface chemistry of carbon xerogels using HNO_3 hydrothermal activation. Carbon 47:1670–1679
30. Stein A, Wang Z, Fierke MA (2009) Functionalization of porous carbon materials with designed pore architecture. Adv Mater 21:265–293
31. Biener J, Stadermann M, Suss M, Worsley MA, Biener MM, Rose KA, Baumann TF (2011) Advanced carbon aerogels for energy applications. Energy Environ Sci 4:656–667
32. Pekala RW (1989) Organic aerogels from the polycondensation of resorcinol with formaldehyde. J Mater Sci 24:3221–3227
33. Fairén-Jiménez D, Carrasco-Marín F, Moreno-Castilla C (2008) Inter- and intra-primary-particle structure of monolithic carbon aerogels obtained with varying solvents. Langmuir 24:2820–2825
34. Gutiérrez MC, Rubio F, del Monte F (2010) Resorcinol-formaldehyde polycondensation in deep eutectic solvents for the preparation of carbons and carbon−carbon nanotube composites. Chem Mater 22:2711–2719
35. Carriazo D, Gutiérrez MC, Ferrer ML, del Monte F (2010) Resorcinol-based deep eutectic solvents as both carbonaceous precursors and templating agents in the synthesis of hierarchical porous carbon monolith. Schem Mater 22:6146–6152
36. Mulik S, Sotiriou-Leventis C, Leventis N (2008) Macroporous electrically conducting carbon networks by pyrolysis of isocyanate-cross-linked resorcinol-formaldehyde aerogels. Chem Mater 20:6985–6997
37. Leventis N, Sotiriou-Leventis C, Chandrasekaran N, Mulik S, Larimore ZJ, Lu H, Churu G, Mang JT (2010) Multifunctional polyurea aerogels from isocyanates and water. A structure-property case study. Chem. Mater. 22:6692–6710
38. Chidambareswarapattar C, Larimore Z, Sotiriou-Leventis C, Mang JT, Leventis N (2010) One-step room-temperature synthesis of fibrous polyimide aerogels from anhydrides and isocyanates and conversion to isomorphic carbons. J Mater Chem 20:6978–9666
39. Wan Y, Qian X, Jia N, Wang Z, Li H, Zhao D (2008) Direct triblock-copolymer-templating synthesis of highly ordered fluorinated mesoporous carbon. Chem Mater 20:1012–1018
40. Sepehri S, García BB, Zhang Q, Cao G (2009) Enhanced electrochemical and structural properties of carbon cryogels by surface chemistry alteration with boron and nitrogen. Carbon 47:1436–1443
41. Hao G-P, Li W-C, Qian D, Lu A-H (2010) Rapid synthesis of nitrogen-doped porous carbon monolith for CO_2 capture. Adv Mater 22:853–857
42. Fang Y, Gu D, Zou Y, Wu Z, Li F, Che R, Deng Y, Tu B, Zhao D (2010) A low-concentration hydrothermal synthesis of biocompatible ordered mesoporous carbon nanospheres with tunable and uniform size. Angew Chem Int Ed 49:7987–7991
43. Liu J, Qiao SZ, Liu H, Chen J, Orpe A, Zhao D, Lu GQ (2011) Extension of the Stöber method to the preparation of monodisperse resorcinol-formaldehyde resin polymer and carbon spheres. Angew Chem Int Ed 50:5947–5951
44. Tien BM, Xu MW, Liu JF (2010) Synthesis and electrochemical characterization of carbon spheres as anode material for lithium-ion battery. Mater Lett 64:1465–1467
45. Horikawa T, Hayashi J, Muroyama K (2004) Size control and characterization of spherical carbon aerogel particles from resorcinol–formaldehyde resin. Carbon 42:169–175

46. Fujikawa D, Uota M, Sakai G, Kijima T (2007) Shape-controlled synthesis of nanocarbons from resorcinol–formaldehyde nanopolymers using surfactant-templated vesicular assemblies. Carbon 45:1289–1295 (Original Research Article)
47. Liu L, Deng QF, Hou XX, Yuan ZY (2012) User-friendly synthesis of nitrogen-containing polymer and microporous carbon spheres for efficient CO_2 capture. J Mater Chem 22:15540–15548
48. Gu JM, Kim WS, Hwang YK, Huh S (2013) Template-free synthesis of N-doped porous carbons and their gas sorption properties. Carbon 56:208–217
49. Liang CD, Hong KL, Guiochon GA, Mays JW, Dai S (2004) Synthesis of a large-scale highly ordered porous carbon film by self-assembly of block copolymers. Angew Chem Int Ed 43:5785–5789
50. Valkama S, Nykänen A, Kosonen H, Ramani R, Tuomisto F, Engelhardt P, Brinke G, Ikkala O, Ruokolainen J (2007) Hierarchical porosity in self-assembled polymers: post-modification of block copolymer-phenolic resin complexes by pyrolysis allows the control of micro- and mesoporosity. Adv Funct Mater 17:183–190
51. Liang CD, Dai S (2006) Synthesis of mesoporous carbon materials via enhanced hydrogen-bonding interaction. J Am Chem Soc 128:5316–5317
52. Saha D, Deng S (2010) Adsorption equilibrium and kinetics of CO_2, CH_4, N_2O, and NH_3 on ordered mesoporous carbon. J Colloid Interface Sci 345:402–409
53. Wang X, Liang C, Dai S (2008) Facile synthesis of ordered mesoporous carbons with high thermal stability by self-assembly of resorcinol-formaldehyde and block copolymers under highly acidic conditions. Langmuir 24:7500–7505
54. Liang C, Dai S (2009) Dual phase separation for synthesis of bimodal meso-/macroporous carbon monoliths. Chem Mater 21:2115–2124
55. Huang Y, Cai H, Feng D, Gu D, Deng Y, Tu B, Wang H, Webley PA, Zhao D (2008) One-step hydrothermal synthesis of ordered mesostructured carbonaceous monoliths with hierarchical porosities. Chem Commun 23:2641–2643
56. Wei J, Zhou D, Sun Z, Deng Y, Xia Y, Zhao D (2013) A controllable synthesis of rich nitrogen-doped ordered mesoporous carbon for CO_2 capture and supercapacitors. Adv Funct Mater 23:2322–2328
57. Liu L, Wang F-Y, Shao G-S, Yuan Z-Y (2010) A low-temperature autoclaving route to synthesize monolithic carbon materials with an ordered mesostructure. Carbon 48:2089–2099
58. Gutiérrez MC, Picó F, Rubio F, Amarilla JM, Palomares FJ, Ferrer ML, Monte F, Rojo JM (2009) PPO_{15}-PEO_{22}-PPO_{15} block copolymer assisted synthesis of monolithic macro- and microporous carbon aerogels exhibiting high conductivity and remarkable capacitance. J Mater Chem 19:1236–1240
59. Zhao X, Wang A, Yan J, Sun G, Sun L, Zhang T (2010) Synthesis and electrochemical performance of heteroatom-incorporated ordered mesoporous carbons. Chem Mater 22:5463–5473
60. Hao G-P, Li W-C, Wang S, Wang G-H, Qi L, Lu A-H (2011) Lysine-assisted rapid synthesis of crack-free hierarchical carbon monoliths with a hexagonal array of mesopores. Carbon 49:3762–3772
61. Hao G-P, Li W-C, Qian D, Wang G-H, Zhang W-P, Zhang T, Wang A-Q, Schüth F, Bongard H-J, Lu A-H (2011) Structurally designed synthesis of mechanically stable poly(benzoxazine-co-resol)-based porous carbon monoliths and their application as high-performance CO_2 capture sorbents. J Am Chem Soc 133:11378–11388
62. Wang Z, Li F, Ergang NS, Stein A (2006) Effects of hierarchical architecture on electronic and mechanical properties of nanocast monolithic porous carbons and carbon−carbon nanocomposites. Chem Mater 18:5543–5553
63. Deng Y, Liu C, Yu T, Liu F, Zhang F, Wan Y, Zhang L, Wang C, Tu B, Webley PA, Wang H, Zhao D (2007) Facile synthesis of hierarchically porous carbons from dual colloidal crystal/block copolymer template approach. Chem Mater 19:3271–3277
64. Xue C, Tu B, Zhao D (2008) Evaporation-induced coating and self-assembly of ordered mesoporous carbon-silica composite monoliths with macroporous architecture on polyurethane foams. Adv Funct Mater 18:3914–3921

65. Wei H, Lv Y, Han L, Tu B, Zhao D (2011) Facile synthesis of transparent mesostructured composites and corresponding crack-free mesoporous carbon/silica monoliths. Chem Mater 23:2353–2360
66. Liu CY, Li LX, Song HH, Chen XH (2007) Facile synthesis of ordered mesoporous carbons from F108/resorcinol–formaldehyde composites obtained in basic media. Chem Commun 7:757–759
67. Feng D, Lv YY, Wu ZX, Dou YQ, Han L, Sun ZK, Xia YY, Zheng GF, Zhao DY (2011) Free-standing mesoporous carbon thin films with highly ordered pore architectures for nanodevices. J Am Chem Soc 133:15148–15150
68. Rodriguez AT, Li XF, Wang J, Steen WA, Fan HY (2007) Facile synthesis of nanostructured carbon through self-assembly between block copolymers and carbohydrates. Adv Funct Mater 17:2710–2716
69. Meng Y, Gu D, Zhang FQ, Shi YF, Yang HF, Li Z, Yu CZ, Tu B, Zhao DY (2005) Ordered mesoporous polymers and homologous carbon frameworks: amphiphilic surfactant templating and direct transformation. Angew Chem Int Ed 44:7053–7059
70. Yoshimune M, Yamamoto T, Nakaiwa M, Haraya K (2008) Preparation of highly mesoporous carbon membranes via a sol–gel process using resorcinol and formaldehyde. Carbon 46:1031–1036
71. Hao G-P, Jin Z-Y, Sun Q, Zhang X-Q, Zhang J-T, Lu A-H (2013) Porous carbon nanosheets with precisely tunable thickness and selective CO_2 adsorption properties. Energy Environ Sci 2013(6):3740–3747
72. Sun X, Li Y (2005) Hollow carbonaceous capsules from glucose solution. J Colloid Interface Sci 291:7–12
73. Li Y, Chen J, Xu Q, He L, Chen Z (2009) Controllable route to solid and hollow monodisperse carbon nanospheres. J Phys Chem C 113:10085–10089
74. Liu J, Qiao SZ, Liu H, Chen J, Orpe A, Zhao D, Lu GQ (2011) Extension of the Stöber method to the preparation of monodisperse resorcinol-formaldehyde resin polymer and carbon spheres. Angew Chem Int Ed 50:5947–5951
75. Wickramaratne NP, Jaroniec M (2013) Activated carbon spheres for CO_2 adsorption. ACS Appl Mater Interfaces 5:1849–1855
76. Wickramaratne NP, Jaroniec M (2013) Importance of small micropores in CO_2 capture by phenolic resin-based activated carbon spheres. J Mater Chem A 1:112–116
77. Wickramaratne NP, Perera VS, Ralph JM, Huang SD, Jaroniec M (2013) Cysteine-assisted tailoring of adsorption properties and particle size of polymer and carbon spheres. Langmuir 29(12):4032–4038
78. Zeng Q, Wu D, Zou C, Xu F, Fu R, Li Z, Liang Y, Su D (2010) Template-free fabrication of hierarchical porous carbon based on intra-/inter-sphere crosslinking of monodisperse styrene–divinylbenzene copolymer nanospheres. Chem Commun 46:5927–5929
79. Jiang P, Bertone JF, Colvin VL (2001) A lost-wax approach to monodisperse colloids and their crystals. Science 291:453–457
80. Lu A-H, Hao G-P, Sun Q (2011) Can carbon spheres be created through the Stöber method? Angew Chem Int Ed 50:9023–9025
81. Wang S, Li W-C, Hao G-P, Hao Y, Sun Q, Zhang X-Q, Lu A-H (2011) Temperature-programmed precise control over the sizes of carbon nanospheres based on benzoxazine chemistry. J Am Chem Soc 133:15304
82. Nakanishi K, Tanaka N (2007) Sol–gel with phase separation. Hierarchically porous materials optimized for high-performance liquid chromatography separations. Acc Chem Res 40:863
83. Brun N, Prabaharan SRS, Morcrette M, Sanchez C, Pécastaings G, Derré A, Soum A, Deleuze H, Birot M, Backov R (2009) Hard macrocellular silica Si(HIPE) foams templating micro/macroporous carbonaceous monoliths: applications as lithium ion battery negative electrodes and electrochemical capacitors. Adv Funct Mater 19:3136
84. Alvarez S, Esquena J, Solans C, Fuertes AB (2004) Meso/macroporous carbon monoliths from polymeric foams. Adv Eng Mater 6:897

85. Yang H, Shi Q, Liu X, Xie S, Jiang D, Zhang F, Yu C, Tu B, Zhao D (2002) Synthesis of ordered mesoporous carbon monoliths with bicontinuous cubic pore structure of Ia3d symmetry. Chem Commun 23:2842
86. Wang X, Bozhilov KN, Feng P (2006) Facile preparation of hierarchically porous carbon monoliths with well-ordered mesostructures. Chem Mater 18:6373–6381
87. Xia Y, Mokaya R (2007) Ordered mesoporous carbon monoliths: CVD nanocasting and hydrogen storage properties. J Phys Chem C 111:10035–10039
88. Taguchi A, Smått J-H, Lindén M (2003) Carbon monoliths possessing a hierarchical, fully interconnected porosity. Adv Mater 15:1209–1211
89. Lu A-H, Smått J-H, Lindén M (2005) Combined surface and volume templating of highly porous nanocast carbon monoliths. Adv Func Mater 15:865–871
90. Lu A-H, Smått J-H, Backlund S, Lindén M (2004) Easy and flexible preparation of nanocasted carbon monoliths exhibiting a multimodal hierarchical porosity. Microporous Mesoporous Mater 72:59–65
91. Shi Z-G, Feng Y-Q, Xu L, Da S-L, Zhang M (2003) Synthesis of a carbon monolith with trimodal pores. Carbon 41:2677–2679
92. Hu Y-S, Adelhelm P, Smarsly BM, Hore S, Antonietti M, Maier J (2007) Synthesis of hierarchically porous carbon monoliths with highly ordered microstructure and their application in rechargeable lithium batteries with high-rate capability. Adv Funct Mater 17:1873–1878
93. Liu N, Yin L, Wang C, Zhang L, Lun N, Xiang D, Qi Y, Gao R (2010) Adjusting the texture and nitrogen content of ordered mesoporous nitrogen-doped carbon materials prepared using SBA-15 silica as a template. Carbon 48:3579–3591
94. Han B-H, Zhou W, Sayari A (2003) Direct preparation of nanoporous carbon by nanocasting. J Am Chem Soc 125:3444–3445
95. Vinu A (2008) Two-dimensional hexagonally-ordered mesoporous carbon nitrides with tunable pore diameter, surface area and nitrogen content. Adv Funct Mater 18:816–827
96. Li Q, Yang J, Feng D, Wu Z, Wu Q, Park SS, Ha CS, Zhao D (2010) Facile synthesis of porous carbon nitride spheres with hierarchical three-dimensional mesostructures for CO_2 capture. Nano Res 3:632–642
97. Nishihara H, Kyotani T (2012) Templated nanocarbons for energy storage. Adv Mater 24:4473–4498
98. Pachfule P, Biswal BP, Banerjee R (2012) Control of porosity by using isoreticular zeolitic imidazolate frameworks (IRZIFs) as a template for porous carbon synthesis. Chem Eur J 18:11399–11408
99. Deng H, Jin S, Zhan L, Wang Y, Lu B, Qiao W, Ling L (2012) Synthesis of porous carbons derived from metal-organic coordination polymers and their adsorption performance for carbon dioxide. New Carbon Mater 27:194–199
100. Almasoudi A, Mokaya R (2012) Preparation and hydrogen storage capacity of templated and activated carbons nanocast from commercially available zeolitic imidazolate framework. J Mater Chem 22:146–152
101. Hu M, Reboul J, Furukawa S, Torad NL, Ji Q, Srinivasu P, Ariga K, Kitagawa S, Yamauchi Y (2012) Direct carbonization of Al-based porous coordination polymer for synthesis of nanoporous carbon. J Am Chem Soc 134:2864–2867
102. Yang SJ, Kim T, Im JH, Kim YS, Lee K, Jung H, Park CR (2012) MOF-derived hierarchically porous carbon with exceptional porosity and hydrogen storage capacity. Chem Mater 24:464–470
103. Chaikittisilp W, Hu M, Wang H, Huang H-S, Fujita T, Wu KC-W, Chen L-C, Yamauchi Y, Ariga K (2012) Nanoporous carbons through direct carbonization of a zeolitic imidazolate framework for supercapacitor electrodes. Chem Commun 48:7259–7261
104. Lim S, Suh K, Kim Y, Yoon M, Park H, Dybtsev DN, Kim K (2012) Porous carbon materials with a controllable surface area synthesized from metal–organic frameworks. Chem Commun 48:7447–7449
105. Ben T, Li Y, Zhu L, Zhang D, Cao D, Xiang Z, Yao X, Qiu S (2012) Selective adsorption of carbon dioxide by carbonized porous aromatic framework (PAF). Energy Environ Sci 5:8370–8376

106. Lee KT, Lytle JC, Ergang NS, Oh SM, Stein A (2005) Synthesis and rate performance of monolithic macroporous carbon electrodes for lithium-ion secondary batteries. Adv Funct Mater 15:547–556
107. Adelhelm P, Hu Y-S, Chuenchom L, Antonietti M, Smarsly BM, Maier J (2007) Generation of hierarchical meso- and macroporous carbon from mesophase pitch by spinodal decomposition using polymer templates. Adv Mater 19:4012–4017
108. Gierszal KP, Jaroniec M (2006) Carbons with extremely large volume of uniform mesopores synthesized by carbonization of phenolic resin film formed on colloidal silica template. J Am Chem Soc 128:10026–10027
109. Zhang S, Chen L, Zhou S, Zhao D, Wu L (2010) Facile synthesis of hierarchically ordered porous carbon via in situ self-assembly of colloidal polymer and silica spheres and its use as a catalyst support. Chem Mater 22:3433–3440
110. Fang B, Kim M-S, Kim JH, Lim S, Yu J-S (2010) Ordered multimodal porous carbon with hierarchical nanostructure for high Li storage capacity and good cycling performance. J Mater Chem 20:10253–10259
111. Liang Y, Liang F, Wu D, Li Z, Xu F, Fu R (2011) Construction of a hierarchical architecture in a wormhole-like mesostructure for enhanced mass transport. Phys Chem Chem Phys 13:8852–8856
112. Meng LY, Park SJ (2012) Influence of MgO template on carbon dioxide adsorption of cation exchange resin-based nanoporous carbon. J Colloid Interface Sci 366:125–129
113. Bhagiyalakshmi M, Hemalatha P, Ganesh M, Mei PM, Jang HT (2011) A direct synthesis of mesoporous carbon supported MgO sorbent for CO_2 capture. Fuel 90:1662–1667
114. Czyèwski A, Kapica J, Moszyński D, Pietrzak R, Przepiórski J (2013) On competitive uptake of SO_2 and CO_2 from air by porous carbon containing CaO and MgO. Chem Eng J 226:348–356
115. Meng L-Y, Park S-J (2012) MgO-templated porous carbons-based CO_2 adsorbents produced by KOH activation. Mater Chem Phys 137:91–96
116. Su F, Zhao XS, Wang Y, Lee JY (2007) Bridging mesoporous carbon particles with carbon nanotubes. Microporous Mesoporous Mater 98:323–329
117. Wang X, Bozhilov KN, Feng P (2006) Facile preparation of hierarchically porous carbon monoliths with well-ordered mesostructures. Chem Mater 18:6373–6381
118. Huwe H, Froeba M (2007) Synthesis and characterization of transition metal and metal oxide nanoparticles inside mesoporous carbon CMK-3. Carbon 45:304–314
119. Wikander K, Hungria AB, Midgley PA, Palmqvist AEC, Holmberg K, Thomas JM (2007) Incorporation of platinum nanoparticles in ordered mesoporous carbon. J Colloid Interface Sci 305:204–208
120. Jang JH, Han S, Hyeon T, Oh SM (2003) Electrochemical capacitor performance of hydrous ruthenium oxide/mesoporous carbon composite electrodes. J Power Sources 123:79–85
121. Kim H, Kim P, Joo JB, Kim W, Song IK, Yi J (2006) Fabrication of a mesoporous Pt-carbon catalyst by the direct templating of mesoporous Pt-alumina for the methanol electro-oxidation. J Power Sources 157:196–200
122. García-Martínez J, Lancaster TM, Ying JY (2008) Synthesis and catalytic applications of self-assembled carbon nanofoams. Adv Mater 20:288–292
123. Long D, Chen Q, Qiao W, Zhan L, Liang X, Ling L (2009) Three-dimensional mesoporous carbon aerogels: ideal catalyst supports for enhanced H_2S oxidation. Chem Commun 26:3898–3900
124. Nielsen TK, Bösenberg U, Gosalawit R, Dornheim M, Cerenius Y, Besenbacher F, Jensen TR (2010) A reversible nanoconfined chemical reaction. ACS Nano 4:3903–3908
125. Worsley MA, Kuntz JD, Cervantes O, Han TY-J, Gash AE, Satcher JH, Baumann TF (2009) Route to high surface area TiO_2/C and TiCN/C composites. J Mater Chem 19:7146–7150
126. Han TY-J, Worsley MA, Baumann TF, Satcher JH (2011) Synthesis of ZnO coated activated carbon aerogel by simple sol–gel route. J Mater Chem 21:330–333
127. Worsley MA, Kucheyev SO, Satcher JH, Hamza AV, Baumann TF (2009) Mechanically robust and electrically conductive carbon nanotube foams. Appl Phys Lett 94:073115

128. Worsley MA, Pauzauskie PJ, Olson TY, Biener J, Satcher JH, Baumann TF (2010) Synthesis of graphene aerogel with high electrical conductivity. J Am Chem Soc 132:14067–14069
129. Worsley MA, Olson TY, Lee JRI, Willey TM, Nielsen MH, Roberts SK, Pauzauskie PJ, Biener J, Satcher J, Baumann TF (2011) High surface area, sp^2-cross-linked three-dimensional graphene monoliths. J Phys Chem Lett 2:921–925
130. Jin Y, Hawkins SC, Huynh CP, Su S (2013) Carbon nanotube modified carbon composite monoliths as superior adsorbents for carbon dioxide capture. Energy Environ Sci 6:2591–2596
131. Qian D, Lei C, Hao G-P, Li W-C, Lu A-H (2012) Synthesis of hierarchical porous carbon monoliths with incorporated metal-organic frameworks for enhancing volumetric based CO_2 capture capability. ACS Appl Mater Interfaces 4:6125
132. Lu A-H, Li W-C, Salabas E-L, Spliethoff B, Schüth F (2006) Low temperature catalytic pyrolysis for the synthesis of high surface area. Nanostruct Graphitic Carbon Chem Mater 18:2086–2094
133. Liang C, Dai S, Guiochon G (2003) A graphitized-carbon monolithic column. Anal Chem 75:4904–4912
134. Fulvio PF, Mayes RT, Wang X, Mahurin SM, Bauer JC, Presser V, McDonough J, Gogotsi Y, Dai S (2011) "Brick-and-Mortar" self-assembly approach to graphitic mesoporous carbon nanocomposites. Adv Funct Mater 21:2208–2215
135. Ghosh A, Subrahmanyam KS, Krishna KS, Datta S, Govindaraj A, Pati SK, Rao CNR (2008) Uptake of H_2 and CO_2 by graphene. J Phys Chem C 112:15704–15707
136. Srinivas G, Burress J, Yildirim T (2012) Graphene oxide derived carbons (GODCs): synthesis and gas adsorption properties. Energy Environ Sci 5:6453–6459
137. Shan M, Xue Q, Jing N, Ling C, Zhang T, Yan Z, Zheng J (2012) Influence of chemical functionalization on the CO_2/N_2 separation performance of porous graphene membranes. Nanoscale 4:5477–5482
138. Zhao Y, Ding H, Zhong Q (2012) Preparation and characterization of aminated graphite oxide for CO_2 capture. Appl Surf Sci 258:4301–4307
139. Koenig SP, Wang L, Pellegrino J, Bunch JS (2012) Selective molecular sieving through porous graphene. Nature Nanotechnol 7:728–732
140. Carrillo I, Rangel E, Magaña LF (2009) Photochemical deposition of Ag nanoparticles on multiwalled carbon nanotubes. Carbon 47:2752–2760
141. Garcia-Gallastegui A, Iruretagoyena D, Gouvea V, Mokhtar M, Asiri AM, Basahel SN, Al-Thabaiti SA, Alyoubi AO, Chadwick D, Shaffer MSP (2012) Graphene oxide as support for layered double hydroxides: enhancing the CO_2 adsorption capacity. Chem Mater 24:4531–4539
142. Zhou D, Liu Q, Cheng Q, Zhao Y, Cui Y, Wang T, Han B (2012) Graphene-manganese oxide hybrid porous material and its application in carbon dioxide adsorption. Chin Sci Bull 57:3059–3064
143. Chandra V, Yu SU, Kim SH, Yoon YS, Kim DY, Kwon AH, Meyyappan M, Kim KS (2012) Highly selective CO_2 capture on N-doped carbon produced by chemical activation of polypyrrole functionalized graphene sheets. Chem Commun 48:735–737
144. Mishra AK, Ramaprabhu S (2012) Nanostructured polyaniline decorated graphene sheets for reversible CO_2 capture. J Mater Chem 22:3708–3712
145. Iijima S (1991) Helical microtubules of graphitic carbon. Nature 354:56–58
146. Nitze F, Hamad EA, Wågberg T (2011) Well-dispersed Pd_3Pt_1 alloy nanoparticles in large pore sized mesocellular carbon foam for improved methanol-tolerant oxygen reduction reaction. Carbon 49:1101–1107
147. Hata K, Futaba DN, Mizuno K, Namai T, Yumura M, Iijima S (2004) Water-assisted highly efficient synthesis of impurity-free single-walled carbon nanotubes. Science 306:1362–1364
148. Yang KS, Edie DD, Lim DY, Kim YM, Choi YO (2003) Preparation of carbon fiber web from electrostatic spinning of PMDA-ODA poly(amic acid) solution. Carbon 41:2039–2046
149. Kowalczyk P, Furmaniak S, Gauden PA, Terzyk AP (2010) Optimal single-walled carbon nanotube vessels for short-term reversible storage of carbon dioxide at ambient temperatures. J Phys Chem C 114:21465–21473
150. Mishra AK, Ramaprabhu S (2012) Polyaniline/multiwalled carbon nanotubes nanocomposite—an excellent reversible CO_2 capture candidate. RSC Adv 2:1746–1750

151. Ye Q, Jiang J, Wang C, Liu Y, Pan H, Shi Y (2012) Adsorption of low-concentration carbon dioxide on amine-modified carbon nanotubes at ambient temperature. Energy Fuels 26:2497–2504
152. Su F, Lu C, Chen H-S (2011) Adsorption, desorption, and thermodynamic studies of CO_2 with high-amine-loaded multiwalled carbon nanotubes. Langmuir 27:8090–8098
153. Lu C, Bai H, Wu B, Su F, Hwang JF (2008) Comparative study of CO_2 capture by carbon nanotubes, activated carbons, and zeolites. Energy Fuels 22:3050–3056
154. Dillon EP, Crouse CA, Barron AR (2008) Synthesis, characterization, and carbon dioxide adsorption of covalently attached polyethyleneimine-functionalized single-wall carbon nanotubes. ACS Nano 2:156–164
155. Liu H, Cooper VR, Dai S, Jiang D (2012) Windowed carbon nanotubes for efficient CO_2 removal from natural gas. J Phys Chem Lett 3:3343–3347
156. Shen W, Zhang S, He Y, Li J, Fan W (2011) Hierarchical porous polyacrylonitrile-based activated carbon fibers for CO_2 capture. J Mater Chem 21:14036–14040
157. Asai M, Ohba T, Iwanaga T, Kanoh H, Endo M, Campos-Delgado J, Terrones M, Nakai K, Kaneko K (2011) Marked adsorption irreversibility of graphitic nanoribbons for CO_2 and H_2O. J Am Chem Soc 133:14880–14883
158. Mantzalis D, Asproulis N (2011) Enhanced carbon dioxide adsorption through carbon nanoscrolls. Phys Rev E84:066304
159. Chmiola J, Largeot C, Taberna PL, Simon P, Gogotsi Y (2010) Monolithic carbide-derived carbon films for micro-supercapacitors. Science 328:480
160. Rose M, Korenblit Y, Kockrick E, Borchardt L, Oschatz M, Kaskel S, Yushin G (2011) Hierarchical micro- and mesoporous carbide-derived carbon as a high-performance electrode material in supercapacitors. Small 7:1108–1117
161. Presser V, McDonough J, Yeon S-H, Gogotsi Y (2011) Effect of pore size on carbon dioxide sorption by carbide derived carbon. Energy Environ Sci 4:3059–3066
162. Qian D, Lei C, Wang E-M, Li W-C, Lu A-H (2013) A method for creating microporous carbons with excellent CO_2 adsorption capacity and selectivity. ChemSusChem. doi: 10.1002/cssc.201300585
163. Zhao Y, Zhao L, Yao KX, Yang Y, Zhang Q, Han Y (2012) Novel porous carbon materials with ultrahigh nitrogen contents for selective CO_2 capture. J Mater Chem 22:19726–19731
164. Nandi M, Okada K, Dutta A, Bhaumik A, Maruyama J, Derks D, Uyama H (2012) Unprecedented CO_2 uptake over highly porous N-doped activated carbon monoliths prepared by physical activation. Chem Commun 48:10283–10285
165. Chen C, Kim J, Ahn W-S (2012) Efficient carbon dioxide capture over a nitrogen-rich carbon having a hierarchical micro-mesopore structure. Fuel 95:360–364
166. Zhao Y, Liu X, Yao KX, Zhao L, Han Y (2012) Superior capture of CO_2 achieved by introducing extra-framework cations into N-doped microporous carbon. Chem Mater 24:4725–4734
167. Zhong M, Natesakhawat S, Baltrus JP, Luebke D, Nulwala H, Matyjaszewski K, Kowalewski T (2012) Copolymer-templated nitrogen-enriched porous nanocarbons for CO_2 capture. Chem Commun 48:11516–11518
168. Stohr B, Boehm HP, Schlogl R (1991) Enhancement of the catalytic activity of activated carbons in oxidation reactions by thermal treatment with ammonia or hydrogen cyanide and observation of a superoxide species as a possible intermediate. Carbon 29:707–720
169. Boehm HP, Mair G, Stoehr T, De Rincon AR, Tereczki B (1984) Carbon as a catalyst in oxidation reactions and hydrogen halide elimination reactions. Fuel 63:1061–1063
170. Przepiórski J, Skrodzewicz M, Morawski AW (2004) High temperature ammonia treatment of activated carbon for enhancement of CO_2 adsorption. Appl Surf Sci 225:235–242
171. Pevida C, Plaza MG, Arias B, Fermoso J, Rubiera F, Pis JJ (2008) Surface modification of activated carbons for CO_2 capture. Appl Surf Sci 254:7165–7172
172. Plaza MG, Rubiera F, Pis JJ, Pevida C (2010) Ammoxidation of carbon materials for CO_2 capture. Appl Surf Sci 256:6843–6849
173. Angeletti E, Canepa C, Martinetti G, Venturello P (1989) Amino groups immobilized on silica gel: an efficient and reusable heterogeneous catalyst for the Knoevenagel condensation. J Chem Soc 1:105–107

174. Yue MB, Chun Y, Cao Y, Dong X, Zhu JH (2006) CO_2 capture by as-prepared SBA-15 with an occluded organic template. Adv Funct Mater 16:1717–1722
175. Zhao L, Bacsik Z, Hedin N, Wei W, Sun Y, Antonietti M, Titirici MM (2010) Carbon dioxide capture on amine-rich carbonaceous materials derived from glucose. ChemSusChem 3:840–845
176. Hwang CC, Jin Z, Lu W, Sun Z, Alemany LB, Lomeda JR, Tour JM (2011) In situ synthesis of polymer-modified mesoporous carbon CMK-3 composites for CO_2 sequestration. ACS Appl Mater Interfaces 3:4782–4786
177. Xia Y, Zhu Y, Tang Y (2012) Preparation of sulfur-doped microporous carbons for the storage of hydrogen and carbon dioxide. Carbon 50:5543–5553
178. Liu Y, Wilcox J (2012) Effects of surface heterogeneity on the adsorption of CO_2 in microporous carbons. Environ Sci Technol 46:1940–1947
179. Babarao R, Dai S, Jiang D (2012) Nitrogen-doped mesoporous carbon for carbon capture—a molecular simulation study. J Phys Chem C 116:7106–7110

http://www.springer.com/978-3-642-54645-7

Porous Materials for Carbon Dioxide Capture

Lu, A.-H.; Dai, S. (Eds.)
2014, X, 245 p. 156 illus., 68 illus. in color., Hardcover
ISBN: 978-3-642-54645-7